J. Fluid Mech. (1986), *vol.* 173, *pp.* 431–471
Printed in Great Britain

Turbulent entrainment: the development of the entrainment assumption, and its application to geophysical flows

By J. S. TURNER

Research School of Earth Sciences, Australian National University, G.P.O. Box 4, Canberra, A.C.T. 2601, Australia

(Received 24 March 1986)

The entrainment assumption, relating the inflow velocity to the local mean velocity of a turbulent flow, has been used successfully to describe natural phenomena over a wide range of scales. Its first application was to plumes rising in stably stratified surroundings, and it has been extended to inclined plumes (gravity currents) and related problems by adding the effect of buoyancy forces, which inhibit mixing across a density interface. More recently, the influence of viscosity differences between a turbulent flow and its surroundings has been studied. This paper surveys the background theory and the laboratory experiments that have been used to understand and quantify each of these phenomena, and discusses their applications in the atmosphere, the ocean and various geological contexts.

1. Introduction

The entrainment hypothesis was first introduced by Sir Geoffrey Taylor in a wartime report on the dynamics of hot gases rising in air. He spoke about it later at a Pacific Science Association meeting in 1949, but did not follow up that talk with a published paper. The idea received a wider exposure through the review lecture by Batchelor (1954), who at that time started two Cambridge students working on theoretical and experimental aspects of the problem, and also revived G.I.'s interest in the subject. This led to the joint publication (Morton, Taylor & Turner 1956, referred to as I in the following sections) which is the more frequently quoted starting point of this subject.

The entrainment hypothesis in its original form can be stated very simply: the mean inflow velocity across the edge of a turbulent flow is assumed to be proportional to a characteristic velocity, usually the local time-averaged maximum mean velocity or the mean velocity over the cross-section at the level of inflow. The total inflow at any position will depend also on the surface area and the geometry and dynamics of the flow – whether it is axisymmetric or two-dimensional, a continuous jet or plume or a suddenly released 'thermal'. In this form the assumption is deceptively simple, and even obvious, since for a jet in uniform surroundings it can be deduced from the similarity solution or justified by the most elementary dimensional considerations. Its power was soon demonstrated, however, by the application to the rise of plumes in stably stratified surroundings, a situation where similarity solutions of the usual kind cannot be applied. It is of course another type of similarity assumption, which implies the same kind of turbulent structure and balance of forces at each height. It can be, and has been, criticized on the grounds that it is demonstrably not exactly true in particular circumstances, and there have been

debates about possible alternative formulations, but it has in fact been enormously successful when applied to phenomena over a very wide range of scales. Though it has been adapted to take account of additional physical processes, the basic assumption remains an effective starting point for quantifying a wide variety of mixing problems.

This paper has several related themes, all of them aimed at demonstrating the power and practical success of the entrainment hypothesis, and reaching a better understanding of why it works so well. The basic definitions and entrainment equations will first be summarized and re-examined in the light of several recent reviews of the fundamentals. The wide range of successful applications to convective phenomena will then be described, with particular emphasis on geophysical examples. These sections on convective flows are followed by a discussion of the extension to mixing processes in stably stratified fluids, first with a mean flow, and then without. Research on the mechanism of the entrainment process, particularly work which sheds light on the role of the large eddies, will be discussed next. Finally, the effect of large viscosity differences on the entrainment mechanism itself is examined. A laboratory study of this aspect was motivated by a geological problem, the mixing of magmas of different composition and physical properties, but it has much wider implications for mixing processes in general.

2. Jets and plumes in a homogeneous environment

In summarizing the present state of the similarity theory, and the measurements used to test it, we will follow the excellent reviews by Fischer *et al.* (1979) and List (1982). They have treated both the axisymmetric and the two-dimensional cases, but only the first will be described here, with emphasis on the comparison between vertically directed turbulent jets (sources of momentum) and plumes (sources of buoyancy) in a uniform environment. Only steady flows will be treated here, not the stage immediately after the flow has been turned on (e.g. 'the starting plume', Turner 1962). A two-dimensional inclined starting plume will, however, be discussed in another context in §6.

The three basic integral properties of these flows (integrated across the cross-sectional area at any level) are the fluxes of mass, momentum and buoyancy. These are defined by:

$$\rho\mu = 2\pi \int_0^\infty \rho w r \, \mathrm{d}r, \tag{1}$$

where μ is the 'specific mass flux' or volume flux, and w is the local mean vertical velocity at radius r from the vertical line above the source;

$$\rho m = 2\pi \int_0^\infty \rho w^2 r \, \mathrm{d}r, \tag{2}$$

where m is the specific momentum flux; and

$$\rho\beta = 2\pi \int_0^\infty \rho w g' r \, \mathrm{d}r, \tag{3}$$

where β is the specific buoyancy flux and $g' = g\Delta\rho/\rho_0$, the effective gravitational acceleration, and ρ_0 is the constant density of the environment.

The symbols Q, M and B are used to denote the initial values of μ, m and β. These three are the primary variables governing the behaviour of axisymmetric turbulent buoyant jets provided that the Reynolds number $M^{\frac{1}{2}}/\nu$ exceeds a few thousand, as

it does in most cases of geophysical interest. When the characteristic linear dimension of the source is small compared with the height of rise, Q soon becomes entirely negligible compared with μ and the flow can be treated as if it arose by supplying M and/or B, but no volume flux, at a point (the virtual source) some distance below the actual source.

The pure jet is defined by M alone, since m remains constant at all distances z. The mean (time-averaged) velocity is self-similar, and is described well by the Gaussian profiles

$$W = W_{\mathrm{m}} \exp\left[-\left(\frac{r}{b_w}\right)^2\right], \tag{4}$$

where W_{m} is the mean velocity on the centreline, and b_w is a radial scale for velocity. The spread of a passive tracer θ (which is assumed now to be so dilute that it has no dynamical effect, though its flux Y is defined by an integral like (3)) is given by

$$\theta = \theta_{\mathrm{m}} \exp\left[-\left(\frac{r}{b_\theta}\right)^2\right]. \tag{5}$$

Dimensional analysis leads immediately to the following forms for the variation of W_{m}, θ_{m}, b_w and b_θ with the overall parameters M and z (the similarity solution):

$$\left.\begin{aligned} W_{\mathrm{m}} &= k_1 M^{\frac{1}{2}} z^{-1}, \\ \theta_{\mathrm{m}} &= k_2 Y M^{-\frac{1}{2}} z^{-1}, \\ b_w &= 0.107 z, \\ b_\theta &= 0.126 z, \end{aligned}\right\} \tag{6}$$

where the constants in the last two relations are experimentally determined values. Note that the spreads of both velocity and tracer are conical with distance z from the source with, however, a wider spread of tracer relative to velocity. (This result, with the same ratio of b_θ/b_w, is also a characteristic feature of plumes, in which the 'tracer', for example temperature, is dynamically active.) The conical form follows from the similarity assumption, regardless of the form of the profiles, but the specific numerical values given in (6) do of course depend on the measured profiles (4) and (5). Measurements of turbulent velocities and tracer-concentration fluctuations show that these also have a self-similar radial distribution, and scale with M and z in a manner consistent with similarity. The constants k_1 and k_2 in (6) can be evaluated using the measured profiles (4) and (5) and the corresponding measurements of turbulence quantities. The value of k_1 computed *ignoring* the axial turbulent flux of momentum (i.e. assuming that all the momentum is carried entirely by the mean flow) is $k_1 = 7.5$, but this is reduced to $k_1 = 6.9$ (in better agreement with the values derived directly from (6)) if the turbulent flux is included. Similar arguments can be applied to the flux of a conserved tracer to give $k_2 = 5.8$; again it has been found that the axial turbulent flux is not zero, and needs to be taken into account to be consistent with the measurements.

It also follows from the definition (1) and the similarity solution for the jet (6) that

$$\mu \propto w b^2 \propto M^{\frac{1}{2}} z \tag{7a}$$

so that

$$\frac{\mathrm{d}\mu}{\mathrm{d}z} = C_{\mathrm{j}} M^{\frac{1}{2}}. \tag{7b}$$

The constant C_{j} for the jet has an experimental value of about 0.25 (Fischer *et al.* 1979). The form (7*a*) implies there is a mean rate of inflow across a circular boundary

(radius b_w, say) which is proportional to z^{-1}, and therefore proportional to the vertical velocity scale W_m given by (6). Thus in this simple case the entrainment relation does *not* require an independent assumption, but it follows from the similarity considerations which led to (6). Moreover, once attention has been concentrated on the inflow velocity, the argument can be turned around: the relations (6) can be regarded as a *consequence* of the simple dimensional assumption that this 'entrainment velocity' should be proportional to the mean (time-averaged) upward velocity W_m (which is the sole velocity scale needed if the flow remains similar).

The corresponding results for pure axisymmetric plumes in homogeneous surroundings, in which B is the conserved quantity, can now be described succinctly in similar terms. In all cases where B is large enough to be of geophysical interest, the flow will become turbulent a small distance above the source, and Q will be negligible, so that all plume properties will depend on B and z. Assuming similar mean profiles (which experimentally are again found to be closely Gaussian) leads to a linear spread and the following similarity solutions for the maximum vertical velocity and the density difference on the axis:

$$\left.\begin{aligned} W_m &= c_1 B^{\frac{1}{3}} z^{-\frac{1}{3}}, \\ g'_m &= c_2 B^{\frac{2}{3}} z^{-\frac{5}{3}}, \end{aligned}\right\} \tag{8}$$

where c_1 and c_2 are constants. The available measurements of turbulent quantities are far fewer for plumes than jets; in particular the magnitude of the axial turbulent fluxes is still uncertain, and so therefore are the precise values of c_1 and c_2. There is no doubt, however, that the levels of turbulent intensity and of concentration fluctuations are much higher in plumes than in jets (Chu, Senior & List 1981).

Related dimensional arguments can be used to write the dependence of μ and m on B and z,

$$m \propto B^{\frac{2}{3}} z^{\frac{4}{3}}, \quad \mu \propto B^{\frac{1}{3}} z^{\frac{5}{3}}.$$

Both of these are now increasing with z, as buoyancy acts to increase the momentum of the flow and entrainment to increase its volume. Eliminating B gives

$$\mu = C_p m^{\frac{1}{2}} z, \tag{9a}$$

where C_p is a constant with an experimentally determined value of 0.25. This is the *same* relation as obtained earlier for the jet, except that the *local* momentum flux m replaces the constant momentum flux M for the jet. Taking into account the dependence of m on z, it follows that for the plume

$$\frac{\mathrm{d}\mu}{\mathrm{d}z} = \tfrac{5}{3} C_p m^{\frac{1}{2}}, \tag{9b}$$

which should be compared with (7*b*). Thus the rates of entrainment into jets and plumes are both defined by the *local* specific momentum flux m, but (since C_p has the same numerical values as C_j in (7*b*)), the experimentally determined coefficient of proportionality (or 'entrainment rate') is higher for plumes. As first pointed out by Batchelor (1954), it follows from the above that for plumes as well as for jets the entrainment relation is a fundamental consequence of the similarity arguments which predict the linear spread of radius with height, and is not an independent assumption.

In the transition regime between jets and plumes, there will therefore be some uncertainty about the entrainment and dilution *rate*, though the *form* of dependence on the integral flow quantities is the same in the two limiting cases. In pratical situations, however, the jet-like region is often small. The initial specific momentum

flux M is continuously being increased by buoyancy, and the buoyancy-generated momentum dominates above a height of order $l_m = M^{\frac{3}{4}}B^{-\frac{1}{2}}$ (Morton 1959). Fischer *et al.* (1979, Chap. 9) have contrasted the behaviour of three flows: a pure jet, a pure plume, and a buoyant jet having the same $M = 3\ \mathrm{m^4\ s^{-2}}$ and $B = 0.26\ \mathrm{m^4\ s^{-3}}$ as the first two. They demonstrated that the 'mixed' case rapidly becomes plume like, with $l_m = 4.5$ m, and that the mean dilution 60 m above the source is $\mu/Q = 68$, which is essentially that for a pure plume (and nearly three times that predicted for the jet).

3. The entrainment equations

The entrainment assumption will now be taken as the explicit starting point, i.e. it will be assumed that the inflow velocity at the 'edge' of the flow is some fraction α of the maximum mean upward velocity. Using the previous notation, this implies that

$$\frac{\mathrm{d}\mu}{\mathrm{d}z} = 2\pi b_w \alpha W_\mathrm{m}, \tag{10}$$

where W_m and b_w for Gaussian profiles are defined by (4). The 'entrainment constant' α clearly depends on the profile chosen, and it will be numerically different if equivalent 'top-hat' profiles are used. Its relation to the constants already given for jets and plumes will be discussed below. The larger spread of the time-averaged mass concentration given in (5) and (6) will also be taken explicitly into account. For both jets and plumes b_θ/b_w has nearly the same constant value, and we write $b_\theta/b_w = \lambda = 1.2$.

The equations of conservation of mass, momentum and buoyancy can be written, using Gaussian profiles and the Boussinesq approximation, in the following form (see Turner 1973 and Fischer *et al.* 1979 for a more detailed discussion of the derivation and underlying assumptions):

$$\left.\begin{aligned} \frac{\mathrm{d}}{\mathrm{d}z}(b_w^2 W_\mathrm{m}) &= 2\alpha b_w W_\mathrm{m}, \\ \frac{\mathrm{d}}{\mathrm{d}z}(\tfrac{1}{2}b_w^2 W_\mathrm{m}^2) &= \lambda^2 b_w^2 g\theta_\mathrm{m}, \\ \frac{\mathrm{d}}{\mathrm{d}z}\left(\frac{\lambda^2 b_w^2 W_\mathrm{m} g\theta_\mathrm{m}}{1+\lambda^2}\right) &= -b_w^2 W_\mathrm{m} N^2(z). \end{aligned}\right\} \tag{11}$$

With the more general application to stratified surroundings in mind, the third (buoyancy) equation includes, on the right, $N^2 = (-g/\rho_1)(\mathrm{d}\rho_0/\mathrm{d}z)$ the square of the local buoyancy frequency. The value of $g' = g\theta = g(\rho_0 - \rho)/\rho_1$ is calculated using the local density difference between the plume ρ and its environment ρ_0 at height z, and ρ_1 is some standard density in the environment. Note again that the numerical coefficients in (11) depend on the form of the profiles, and the velocity and length scales used; they are different for 'top-hat' profiles. The equations can be solved once initial values of b_w, W_m and θ_m are specified, as they can be if Q, M and B are known.

For homogeneous surroundings ($N^2 = 0$), the similarity solutions are entirely equivalent to (11), and will in fact be particular solutions of these equations. For the limiting cases of jets and plumes Fischer *et al.* (1979) have used the experimentally determined parameters to show that (for Gaussian profiles)

$$\alpha_\mathrm{jets} = 0.054, \quad \alpha_\mathrm{plumes} = 0.083. \tag{12}$$

This difference in entrainment rates for jets and plumes is consistent with the deductions made from (9*b*), which indicated that the dilution rate of a plume is higher than for a jet for the same local momentum flux. Turner (1973, p. 173) presented earlier evidence for different α-values (obtained by Ricou & Spalding 1961), but suggested using caution until further evidence became available. This has now been obtained and assessed, and use of (12) does seem justified.

Another point worth repeating is that the values of α given by (12) are only indirectly related to the angle of spread of the velocity profile in jets and plumes. For jets, (10) gives $\mathrm{d}b_w/\mathrm{d}z = 2\alpha = 0.107$, as already set out in (6). For plumes, the corresponding relation is $\mathrm{d}b_w/\mathrm{d}z = \frac{6}{5}\alpha = 0.100$, although this value is based on much less precise data. Thus the angles of spread are very little different for jets and plumes, in spite of the fact that the 'entrainment rates' as defined above are substantially different. A constant angle of spread was suggested as a reasonable fit to all the experimental results on buoyant jets over the whole length of the flow, including the transition (List & Imberger 1973), though Chu *et al.* (1981) have reported anomalously small angles of spread in the transition region.

Note again that α does not enter very sensitively into many calculations, so that using a fixed value (that for the plume seems most appropriate, though even an arbitrary compromise between the values given in (12) is a possible choice) will not make a large practical difference to the final answer. Relating entrainment to W_m and therefore to the largest scales of motion in a jet or plume seems to be the physically most significant step. This assumption works so well because in fact the initial mechanism of entrainment, which will be discussed in more detail in §8, is the engulfing of external fluid by the large eddies at the edge of a jet or plume. The assumption of similarity means that these large eddies retain the same relation to the mean flow whatever the scale of motion, and the level of turbulent energy at smaller scales is less important. The external parameters (like B) defining the flow vary over such a wide range that provided the mean flow scales with these in the manner predicted by similarity, the smaller variations of α will be relatively insignificant.

Hunt, Rottman & Britter (1983) have pointed out that several different usages of the term 'entrainment velocity' have grown up over the past thirty years. Though they are conceptually and sometimes quantitatively different, they are sometimes confused, and before moving on to more complicated topics it is worth discussing and comparing them carefully, using the simple jet as an example. The first use is the definition that we have set out in (10); the entrainment velocity E is the rate $E = \alpha W$ at which external fluid flows into the turbulent flow across its boundary.

A second definition is related to the rate E_b at which the edge of a turbulent flow is spreading out and engulfing the surrounding fluid at rest. For a planar interface (such as those discussed in §7) E and E_b are just equal and opposite, but this is not true in other geometries. For a jet, $M \propto b^2w^2$ is constant, so (10) implies that $\mathrm{d}b/\mathrm{d}z = 2\alpha$. Conceptually it is easier to think in terms of 'top-hat' profiles, or velocities averaged across the section, and in this context W and b are used to denote the velocity and radius defined in this way. The outward velocity at the 'edge' of the jet, measured in a fixed coordinate system, is

$$\begin{aligned} E_b &= -\frac{\mathrm{d}b}{\mathrm{d}z}W \\ &= -2\alpha W \\ &= -2E. \end{aligned} \tag{13a}$$

A third entrainment velocity E_b^* can be defined if the outward velocity is measured relative to the local mean flow, leading to

$$E_b^* = E_b - E = -3E. \tag{13b}$$

Entrainment can also be defined in terms of the rate of transfer of a contaminant across a fixed surface (for example in a two-layer stratified system, with turbulence on both sides of an interface). The flux entrainment velocity $E_F = F_c/\Delta C$, where F_c is the flux of concentration (or density) and ΔC is the concentration difference, is independent of ΔC. Note that E_F may be in the opposite direction to E_b, and that E_F can be non-zero while E and E_b are both zero.

4. Plumes in stable surroundings, and further extensions

We now turn to the problem that first demonstrated the more general applicability of the entrainment assumption and the use of the entrainment equations (11). When the environment is stably stratified, the ordinary similarity solutions in powers of the height are not appropriate, because in these circumstances plumes must come to rest at a finite height. They entrain denser fluid during the early part of their rise and reach a terminal height where their density equals that of their surroundings and they spread out horizontally. There is no comparable limitation on the entrainment equations (11), which can be integrated from $z = 0$ for any initial values of b_w, W_m and θ_m, corresponding to arbitrary Q, M and B. The practically most useful asymptotic case is still that for a virtual point source of buoyancy alone in an environment with constant N. The entrainment equations can then be put in a non-dimensional form using B and N as the two governing parameters that determine the scale of the motion. The transformations relating the dimensional and dimensionless variables (the latter denoted by a subscript 1) were first given in I; with the simplifying assumption $\lambda = 1$, they are

$$\left.\begin{aligned} z &= 0.410\alpha^{-\frac{1}{2}}B^{\frac{1}{4}}N^{-\frac{3}{4}}z_1, \\ b_w &= 0.819\alpha^{\frac{1}{2}}B^{\frac{1}{4}}N^{-\frac{3}{4}}b_1, \\ W_\mathrm{m} &= 1.158\alpha^{-\frac{1}{2}}B^{\frac{1}{4}}N^{\frac{1}{4}}w_1, \\ \theta_\mathrm{m} &= 0.819\alpha^{-\frac{1}{2}}B^{\frac{1}{4}}N^{\frac{5}{4}}\theta_1. \end{aligned}\right\} \tag{14}$$

The corresponding dimensionless equations will not be repeated here, but the solutions of them set out in I, for b_1, w_1 and θ_1 as functions of z_1, are shown in figure 1. Up to $z_1 = 2.0$ the plume spreads nearly linearly, and the solutions are close to those in a uniform environment. Above this height, it spreads more rapidly sideways; at $z_1 = 2.13$ the density difference first vanishes, and at $z_1 = 2.80$ the vertical velocity vanishes. These two dimensionless heights give plausible estimates of the bottom and top of the horizontally spreading region of flow, though in this region of rapid spreading the entrainment formulation based on similarity of the profiles becomes more questionable, and the overshoot that is observed is not properly represented. When the maximum value of z_1 and the value of α previously determined for a uniform environment ($\alpha = 0.083$) are substituted into the first of equations (14), one obtains a *numerical* estimate for z_max in terms of B and N.

Of course, the *form* of the relation for z_max in powers of these two parameters can be written immediately using a dimensional argument, without any explicit reference to (11) or to (14). Once this relation is accepted, the multiplying constant can be

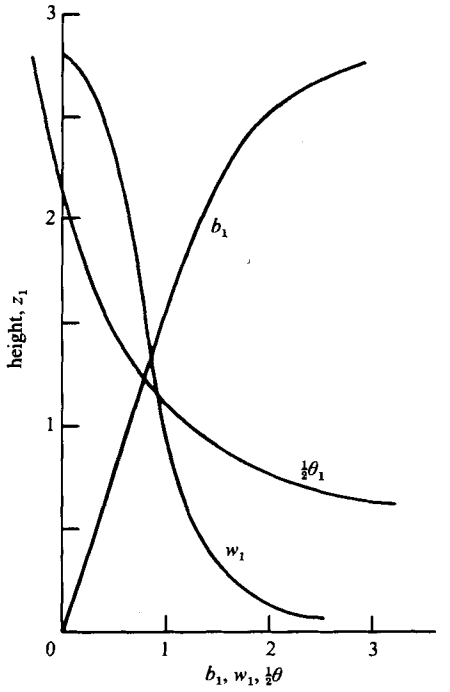

FIGURE 1. The dimensionless solutions for the radius b_1, velocity w_1 and buoyancy θ_1 of a plume in stratified surroundings, defined by (14), plotted as a function of height z_1.

evaluated by direct experiment, as was done in I using small-scale experiments in stratified salt solution such as that shown in figure 2 to give

$$z_{\max} = 5.0F^{\frac{1}{4}}G^{-\frac{3}{8}}$$

$$= 3.8B^{\frac{1}{4}}N^{-\frac{3}{4}}, \tag{15}$$

where (following Briggs 1969) we have used the notation $F = B/\pi$ and $G = N^2$. There is a great deal of physics hidden in this formula, however, and the underlying requirements for it to be valid (flow similarity at each cross-section, and the dependence of entrainment on the largest scales of motion), are not apparent from (15) alone. Nevertheless, the numerical constant in (15) is a measure of the average rate of entrainment over the whole height of rise, and the direct laboratory evaluation using as wide a range of N and B as possible is probably the most satisfactory method of determining this constant.

This method has certainly been amply justified by subsequent results obtained in many different contexts. Briggs (1969) compiled the data shown in figure 3(*a*) (and quoted by Turner 1973) which shows that the same formula (15), with the *same* numerical constant, can be applied to plumes extending up to 10000 ft (3 km) above an oil fire. (For the atmosphere, potential temperature gradients must of course be used in determining N.) Since then, the height range has been extended by another order of magnitude; Wilson *et al.* (1978) have successfully applied (15) to describe the heights of rise of the plumes of hot gas and ash emitted from erupting volcanoes, and the model has been further developed by Sparks (1986). They assumed a standard atmospheric lapse rate, and related the heat output to the equivalent volume eruption rate of lava (with allowance for a reduced efficiency of transfer of

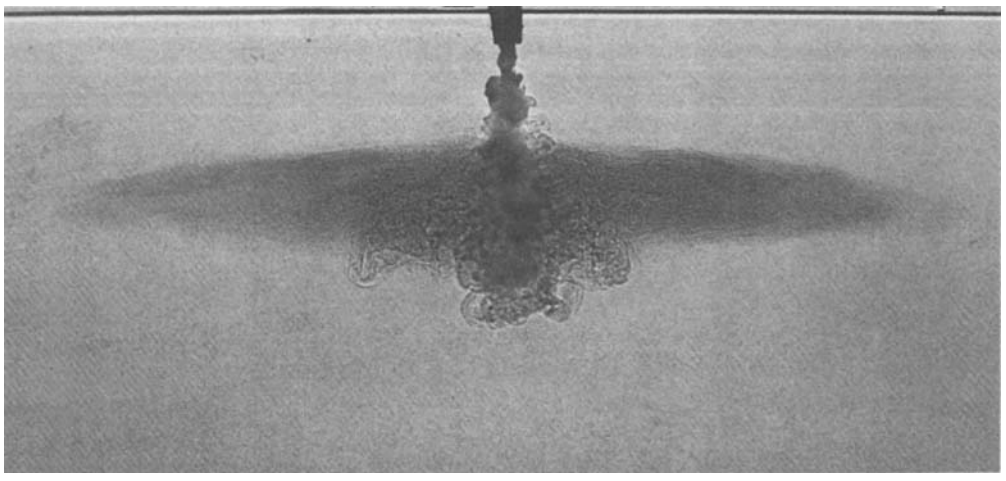

FIGURE 2. Shadowgraph picture of a dyed, turbulent plume of salt solution spreading out in stratified surroundings at the level where its density equals that of the environment (about 10 cm in this laboratory experiment). Note the overshoot to the level where the velocity vanishes.

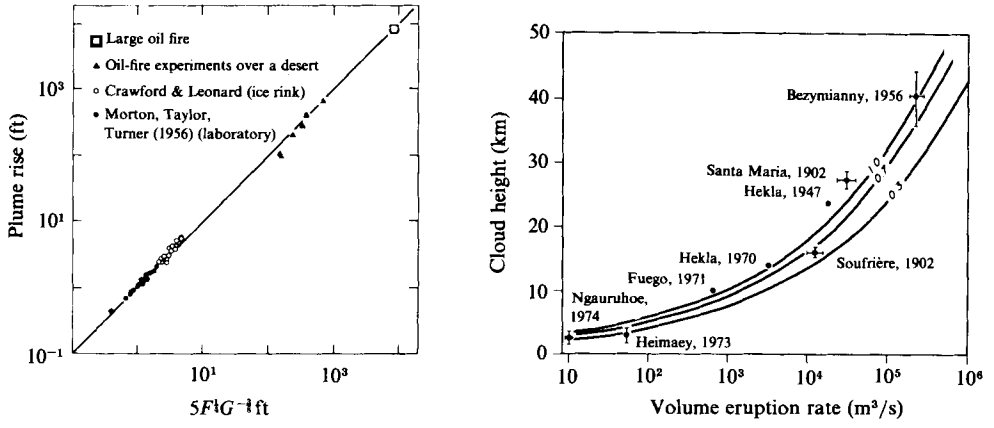

FIGURE 3. The extrapolation to large scales of laboratory results on the rise of plumes in stratified surroundings. (*a*) The data compiled by Briggs (1969), compared with (15). (*b*) Heights of volcanic clouds plotted against volume eruption rates (Wilson *et al.* 1978). Three theoretical curves are shown for different 'efficiencies' (the fraction of the heat associated with the hot rock which is transferred to the air to drive convection). Again (15) has been used, with a standard atmospheric lapse rate.

heat to the plume due to the falling out of the larger hot rock particles near the vent). Their plot of observed cloud heights as a function of eruption rate for eight large eruptions is shown in figure 3(*b*), where the observations are compared with (15) (using three different 'efficiency factors'). Figure 4 is a photograph of the rising and spreading plume for the 1956 Bezymianny eruption, which is probably the largest natural event to which this theory has been applied.

Before giving other recent engineering and geophysical examples, it is worth pausing again to consider why (15) works as well as it does, given the many simplifying assumptions that it implies, and the factors that have been neglected. The volcanic source has a finite area, and the flow is undoubtedly jetlike at the exit:

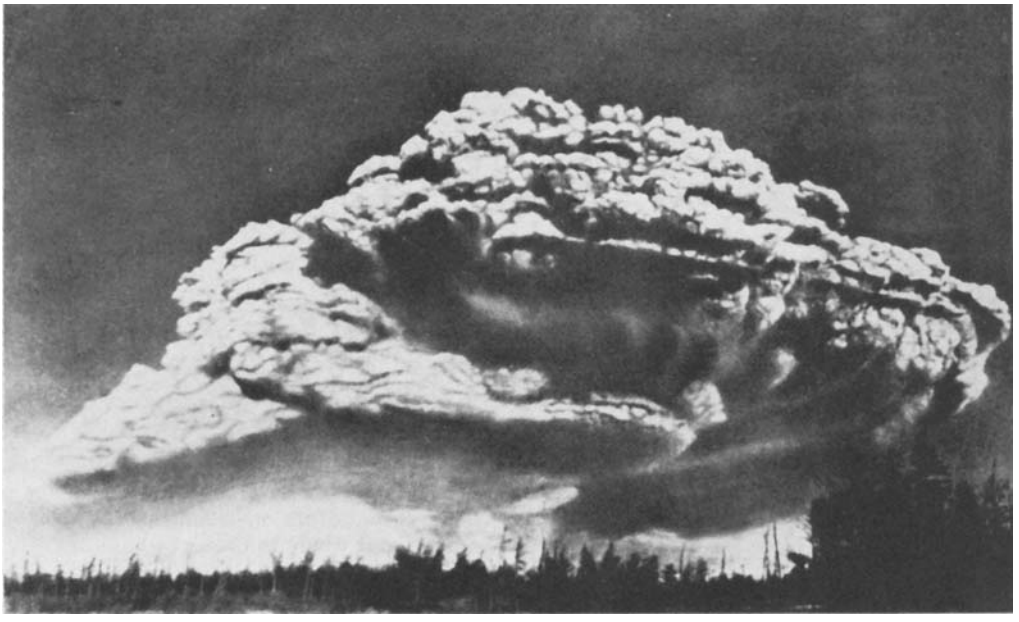

FIGURE 4. The rising and spreading plume above the Bezymianny eruption of 1956 (from Gorshkov 1959). This is the largest natural event to which the plume theory, and the extrapolation of the laboratory data, has been applied.

but our discussion of buoyant jets in homogeneous surroundings has shown that both these starting conditions are 'forgotten' within say ten diameters above the source. The density gradient or N^2 is not strictly constant, with height or in different geographical regions, but the total variation is small, and it enters weakly into (15). As discussed previously, α too has such a small variation between various types of turbulent flows that is it plausible to use a constant value (and furthermore the square root enters into (14)). In fact the only parameter that varies substantially is B and this does so by an enormous factor of 10^{20} between the laboratory and the largest-scale natural flow. What all the observations have shown convincingly is that the height of rise of plumes in a stable atmosphere is predicted to acceptable accuracy by $z_{\max} \propto B^{\frac{1}{4}}$, which follows from the entraining plume dynamics, with the near constancy of the numerical factor being an indication of the insensitivity to all the other parameters.

When the conditions at the source are well enough known, and significantly different from the relations appropriate for pure plumes from point sources, or the environmental density gradient varies greatly over the height of interest, it is possible to integrate the set of equations (11) directly including the initial momentum and the detailed form of $N^2(z)$. This is sometimes justified in engineering contexts, for example to predict the height of rise sewage effluent above outfalls on the sea floor.

Another application, in which the finite area of the source certainly needs to be taken into account, is the rise and growth of large convective clouds. The use of the entrainment equations in this context was initiated by Morton (1957) and followed up by Squires & Turner (1962). By adding a moisture-conservation equation to the other three and allowing for the generation of extra buoyancy by the release of latent heat, they produced results with some features in good agreement with observation,

especially their prediction of cloud shapes as the upflow first accelerates and narrows just above cloudbase and then spreads out in stable surroundings. However, it was not possible to predict both realistic liquid-water concentrations and heights of penetration for the same cloud, and it seems that clouds, which are often nearly as broad as they are tall, cannot properly be described by similarity theories which imply lateral entrainment and a fully developed state at each cross-section.

Other problems of engineering importance involve jets and plumes discharged at an angle to the vertical, or into a cross-flow with or without stratification. These have also been solved using extensions of the dimensional arguments or similarity solutions developed from the equations of motion to describe sections of the flow where particular processes dominate. (Refer again to Fischer *et al.* 1979 and List 1982).

There have also been several recent geological applications of plume theory. The maximum height of rise of the hot-water plumes above individual 'black-smoker' vents at spreading centres has been calculated by Campbell, McDougall & Turner (1984) (using (15) with estimates of the flow rate and the density gradient) to be about 300 m, in satisfactory agreement with the observed height to which tracer ^{3}He from the vents rises above the East Pacific Rise. The corresponding flow velocities are so much greater than the fall velocities of the small sulphide particles (the 'black smoke') that this cannot be deposited locally from the plume, and other mechanisms need to be considered to explain the build-up of massive sulphide deposits. More accurate estimates of the dispersion will, of course, need to take account of the effect of currents in bending the plumes over and the interaction of many small plumes to form a larger distributed source.

Campbell, Naldrett & Barnes (1983) have applied plume theory to describe the behaviour of new inputs of less dense magma injected into a stratified magma chamber – a very different fluid system from air or aqueous solutions! They set out to explain the origin of platinum-rich sulphide horizons in large igneous intrusions, starting with the principle (derived from geochemical considerations) that a large amount of mixing between an incoming pulse of sulphide melt and the Pt dispersed through the original magma is essential if Pt is to be concentrated into sulphide ore. The most favourable conditions for producing such mixing, they have argued, occur when two conditions are met. First, the new hot magma rises as a plume, mixes with the host magma and spreads laterally to form a layer at its own density level. (For this stage, they have calculated the entrainment into line plumes of various strengths, and the dilutions at different heights.) Secondly, the intruded layer can lose heat rapidly to the cooler overlying host magma. If the density difference (due to the combined effect of temperature and composition) between the original magmas is small, and so is the density gradient, then the lower part of the magma chamber will destabilize and convect as it cools, allowing any immiscible sulphides that form to equilibrate with a large volume of silicate melt.

5. Turbulent thermals and buoyant vortex rings

Suddenly released buoyant clouds or thermals have also been studied using an entrainment hypothesis and set of entrainment equations, following the formulation of this idea in I. There is, however, a significant difference between the thermal and the plume cases which was discussed by Turner (1973), and this is worth summarizing again in the present context.

The equations of conservation of mass, momentum and buoyancy analogous to (11) are for a spherical thermal

$$\left.\begin{aligned} \frac{\mathrm{d}b^3}{\mathrm{d}t} &= 3\alpha b^2 w_0, \\ \frac{\mathrm{d}(b^3 w_0)}{\mathrm{d}t} &= \tfrac{2}{3} b^3 g', \\ \frac{\mathrm{d}(b^3 g')}{\mathrm{d}t} &= -b^3 w_0 N^2. \end{aligned}\right\} \tag{16}$$

In writing these equations, with the specific numerical constants given, it has been assumed that the inflow velocity into a thermal is proportional to the mean upward velocity w_0 and to the surface area, and that the virtual-mass coefficient, describing the momentum of surrounding fluid, is that appropriate to a sphere. The Boussinesq assumption is also implied; the modifications introduced by including large density differences in the inertia terms were added by Escudier & Maxworthy (1973), and these will be discussed further in §8.

The first of these equations shows immediately that $b = \alpha z$, so that the entrainment assumption, used with mass continuity alone, implies that the spread is linear with height regardless of the properties of the environment. This is very different from the result for plumes. The first two equations in (11) are needed to derive an expression for $\mathrm{d}b_w/\mathrm{d}z$, which depends not only on α but also on the local values of b_w, W_m and θ_m. The examples given in §4 have indicated that the shape of a plume which first accelerates and then decelerates in stably stratified surroundings can be very far from linear.

Similarity solutions equivalent to (8) and (15) can be written to describe respectively the motion and dilution in homogeneous surroundings, and the final height attained in a linearly stratified environment. The latter, for example, may be expressed as

$$z_\mathrm{max} \propto \alpha^{-\frac{3}{4}} F_*^{\frac{1}{4}} N^{-\frac{1}{2}} = 2.66 F_*^{\frac{1}{4}} G^{-\frac{1}{4}}, \tag{17}$$

where F_* is the total buoyancy released at the source ($F_* = g(\rho_0 - \rho) V_0/\rho_0$ where ρ and V_0 are the initial density and volume of source fluid), and the constant is taken from the laboratory experiments reported in I. Thermals released from rest are observed to spread at a much wider angle than plumes, and thus they dilute more rapidly with height. The angle of spread is also more variable than it is for plumes and is sensitive to the initial conditions. This behaviour, and other important properties of thermals, can be understood better if they are regarded as a special case of a buoyant vortex ring, following Turner (1957, 1960).

For a thermal, the circulation is generated by buoyancy, whereas in a vortex ring the buoyancy F_* and circulation $K_0 \propto W_0 R$, where R is the radial distance from the axis to the centre of the core, can be specified independently at the source. For rings with sharp cores containing all the buoyancy and vorticity, both of these quantities remain constant in time in a uniform environment, since a circuit can be taken round the core entirely in fluid of constant density. Buoyancy acts, however, to increase the momentum of the vortex ring and the surrounding fluid which is set into motion by its passage. This momentum, or total impulse P, is defined by $P = \pi\rho K_0 R^2$, and the momentum equation becomes

$$\frac{\mathrm{d}P}{\mathrm{d}t} = \pi\rho K_0 \frac{\mathrm{d}R^2}{\mathrm{d}t} = \rho F_*. \tag{18}$$

Integrating gives $R^2 - R_0^2 = F_* t/\pi K_0$, and adding the assumption that the velocity distribution remains similar at all heights, so that $w_0 = CK_0/R$, leads to

$$R = \alpha_R z = \frac{F_*}{2\pi C K_0^2} z. \tag{19}$$

Thus the angle of spread of a buoyant vortex ring is constant and proportional to F_*/K_0^2. Generation of circulation in a buoyant thermal following the release of fluid having a small density difference from its surroundings produces a relatively small value of K_0 and large α_R. K can remain constant in this case too if the generation of circulation by buoyant fluid up the centre is balanced by its destruction due to the mixing across the centreline of vorticity of opposite signs. Increasing K_0 for a given F_* (by injecting fluid with extra momentum at the source), leads to a smaller angle of spread. This can also be achieved by the action of buoyancy in the early stages of rise when the density differences are large; this process can also lead to the formation of a distinct, persistent hot core (see figure 5). Once a stable† similarity state is attained F_*/K_0^2 stays constant, and defines the rate of mixing with the environment.

Thus the total rate of addition of external fluid is determined by the overall dynamics, through the momentum equation (18) and the initial conditions, and without considering turbulence or indeed any detailed mixing mechanism. It is questionable, therefore, whether it is really appropriate to regard this as an 'entrainment' process at all, in the sense that this concept has been used for jets and plumes. Nevertheless, (16) and (18), and the generalized version of these (Turner 1960) which allows for the variation of K with height and of α (or α_R) with K_0, are useful in describing the rise of buoyant thermals or vortex rings in different circumstances, particularly in stable surroundings. An indication of the overall effect on the height of rise may be obtained by substituting the form $\alpha \propto F_*/K_0^2$ from (19) into (17) which gives

$$z_{\max} \propto F_*^{-\frac{1}{2}} K_0^{\frac{3}{2}} G^{-\frac{1}{4}}. \tag{20}$$

Note the very strong dependence of height on K_0, which implies that relatively modest changes in the initial circulation can lead to a large increase in the final height to which buoyant material will rise in stable surroundings; this effect was certainly observed for the large explosion clouds pictured in figure 5. The surprising prediction that $z_{\max}$ *decreases* with increasing F_* for fixed K_0 has been confirmed by laboratory experiments; this behaviour is a consequence of the larger angle of spread, and increased rate of entrainment of the denser environment, corresponding to a larger F_*/K_0^2. Near the final height in stable surroundings, the similarity assumption with constant α and rate of spreading is not a good representation of the behaviour. Only in special circumstances can the radius continue to increase linearly, as implied by (16). For a buoyant vortex ring in which the circulation remains non-zero when the momentum vanishes, the radius begins to decrease soon after the buoyancy becomes zero, and the vortex ring will therefore tend to collapse suddenly and mix into its surroundings.

It is also interesting to consider thermals in unstable surroundings or (equivalently) those in which buoyancy is generated internally, so that the density difference is changing in a prescribed way. Using chemically generated gas bubbles in a liquid to simulate the release of latent heat in atmospheric clouds, Turner (1963) produced laboratory thermals which either accelerated uniformly, or rose with constant

† If the core becomes unstable, however, there could be a rapid breakdown to a turbulent state, and degeneration into a thermal with a much smaller value of K.

FIGURE 5. The buoyant vortex ring formed by a large explosion, showing the hot core and the surrounding fluid, marked by dust, which is moving with the ring.

velocity. In all cases the radius increased linearly with distance, as predicted by similarity theory. There was a small change in the mean half-angle of spread which ranged from $\alpha = 0.20$ for accelerating thermals, through $\alpha = 0.23$ for elements with constant velocity to 0.25 (or slightly more) for ordinary thermals with constant total buoyancy.

A. D. McEwan (personal communication) has also produced experimental thermals and plumes in which the buoyancy is increasing because of the release of gas bubbles. His technique uses the pressure change with decreasing depth to produce bubbles from a saturated liquid, and is therefore a better model of the release of latent heat by condensation. (It also allows the process to be reversible and simulate evaporation.)

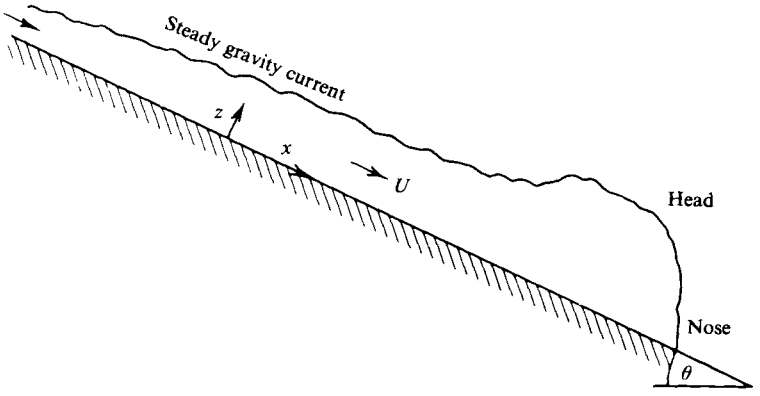

FIGURE 6. Sketch of a gravity current on a slope, with an initial head followed by a steady layer flow. Entrainment into this inclined two-dimensional plume is inhibited by the component of gravity acting normal to the edge.

He has observed that plumes with internally generated buoyancy do not entrain as rapidly as normal plumes, and has attributed this to the fact that this process reduces the toroidal circulation and hence the strength of the entraining eddies.

6. Turbulent gravity currents

There have been two recent reviews of gravity currents, covering both the fundamentals and the increasingly diverse range of applications, which should be mentioned here, and consulted for further details of these flows. That by Simpson (1982) concentrates on horizontal currents, occurring either at the top or bottom boundary of a fluid or as intrusions at some intermediate level in a stratified environment. In these cases mixing at the front is generally more important than the direct mixing into the steady flow behind, and the front is a controlling feature of the flow. Hopfinger's (1983) review, on the other hand, addresses the problem of avalanches, and therefore deals with inclined gravity currents in more detail. It is the latter problem to which the extension of the entrainment ideas has been explicitly and successfully applied, and which will be discussed in this section before outlining the wide-ranging applications to natural phenomena.

A turbulent gravity current on a sloping floor or roof can be regarded as a special case of a two-dimensional plume (figure 6). Again the mean flow is driven by gravity, or more precisely the component of gravity acting down the slope. There will also be a component of gravity acting normal to the entraining edge of the plume, so that buoyancy forces have the extra effect of inhibiting mixing into the plume. For a strictly two-dimensional flow over a plane boundary, with a homogeneous environment at rest, the equations of conservation of mass and momentum (corresponding to the first two of the entrainment equations (11)) are

$$\frac{\mathrm{d}(Uh)}{\mathrm{d}x} = EU, \quad \frac{\mathrm{d}(U^2h)}{\mathrm{d}x} = g'h\sin\theta. \tag{21}$$

Here U is the mean velocity in the direction x along the slope, and h is the depth defined by integrals across the flow in the direction of the normal z:

$$Uh = \int_0^\infty \mathrm{d}z, \quad U^2h = \int_0^\infty u^2\,\mathrm{d}z,$$

$g' = g\Delta\rho/\rho$, θ is the slope, and E is an entrainment parameter which will be discussed below. In writing the second equation, the boundary friction has been neglected compared with the drag due to mixing, an assumption which can readily be justified for steep slopes. It should be noted, however, that the case where θ is small, and bottom friction is significant, is the important one for lakes and for bottom currents in the ocean. (Refer again to Fischer *et al.* 1979).

According to (21) the inflow or entrainment velocity is still assumed to be proportional to the local mean velocity of the flow, so that the basic entrainment hypothesis remains unchanged. What has been added is the assumption, following Ellison & Turner (1959), that E is no longer a constant, but that it should be taken to be a function $E(Ri_0)$ of an overall Richardson number defined by

$$Ri_0 = \frac{g'h\cos\theta}{U^2} = \frac{A\cos\theta}{U^3}, \tag{22}$$

where $A = g'hU$ is the (constant) buoyancy flux per unit width. Thus a new physical parameter has been introduced, representing the stabilizing effect of the density difference and the relative importance of buoyancy and inertial forces, but the dominance of entrainment by the large-eddy structure is still implied by this formulation.

The solution of (21) is equivalent to the similarity solution for a two-dimensional plume with source strength A per unit width. On a given slope, the mean velocity is constant with distance x and proportional to $A^{\frac{1}{3}}$, and for slopes $\geqslant 5°$ the speed is very insensitive to slope. When the unsteady 'starting-plume' phase of the motion is considered (figure 6), as it must be in the application to avalanches, for example, the front velocity U_f has the same form $U_f \propto cA^{\frac{1}{3}}$ (Britter & Linden 1980). The multiplying constant c is 1.5 ± 0.2 for $5° \leqslant \theta \leqslant 90°$, and this front velocity is about 60 % of the mean velocity of the steady flow behind (when the density differences are small). The angle of spread of the steady current is constant along the slope, and $\mathrm{d}h/\mathrm{d}x = E(Ri_0)$, a result that continues to be valid when bottom friction is taken into account. Thus Ri_0 and E have particular values corresponding to a given slope; the flow adjusts to the equilibrium value quite rapidly. E is a strong function of Ri_0, which was measured by Ellison & Turner (1959) and can be represented to good accuracy by

$$E = \frac{0.08 - 0.1Ri_0}{1 + 5Ri_0}. \tag{23}$$

The same set of experiments showed that $E \approx 10^{-3}(\theta + 5)$, where θ is in degrees, whereas the head grows at the much faster rate $\mathrm{d}H/\mathrm{d}x \approx 4 \times 10^{-3}\,\theta$. For a vertical two-dimensional starting plume the spread of the head is still very much larger than that of the plume behind, whereas for an axisymmetric starting plume the two remain more nearly equal. The two-dimensional-plume theory can be extended to flows down a slope in a stratified environment. The expression corresponding to (15), for the depth $z_{\max}$ at which a two-dimensional current will reach the density of its surroundings and spread out away from the slope into the interior, is

$$z_{\max} \propto E^{-\frac{1}{3}}A^{\frac{1}{3}}N^{-1}. \tag{24}$$

Hopfinger (1983) has also reviewed the related work on two-dimensional thermals or buoyant cloud moving along a slope. These have features in common with the head of a gravity current, except that they are not supplied with buoyant fluid from behind. The shape can be approximated by a half-ellipse; clouds released from rest

first accelerate and then decelerate, and in the decelerating phase their velocity as a function of position x_f down the slope is described by the result obtained from a dimensional argument. This is $U_f \sim (g'_0 V_0/x_f)^{\frac{1}{2}}$, where V_0 is the initial volume per unit width and g'_0 the initial buoyancy. The multiplying constant is now much more sensitive to slope angle, and it decreases as the slope tends to 90°, reflecting a large increase in the mixing rate in that limit. Over the range $5° \leqslant \theta \leqslant 50°$, which is most important for avalances, however, the front velocity is given by $U_f = (2.6 \pm 0.2)\,(g'_0 V_0/x_f)^{\frac{1}{2}}$.

One of the early applications of this entrainment theory of gravity currents was to methane roof layers in coal mines (this provided the motivation for the experiments of Ellison & Turner 1959). The above results for an environment at rest can also be extended to calculate the opposing (non-turbulent) flow that would be needed to prevent a dangerous layer of methane flowing uphill along the roof of a sloping mine roadway. The entrainment rate is now assumed to be proportional to the *difference* in velocity across the edge of the roof layer, and Ri_0 is defined using this velocity difference. When the opposing (downslope) ambient flow reaches a certain critical speed, there can be a sudden decrease in Ri_0, leading to a reversal of the layer flow associated with a greatly increased rate of mixing and hence dilution of the methane layer.

Longuet-Higgins & Turner (1974) have shown that several features of a spilling breaker on the surface of shoaling water can be described using a similar model which regards the whitecap as a turbulent plume, running down the forward slope of the wave and entraining laminar, upward-moving fluid below it. In particular they predicted the conditions under which the whitecap can form and survive (which depends sensitively on the slope) and the magnitude of the downslope velocity, in good agreement with laboratory observations.

Another straightforward application is to katabatic winds formed by cooling at a slope (on the Antarctic continent, for example). In this case the strength of the onshore wind needed to bring the air to rest near the ground can be calculated. A more recent spectacular large-scale application of these ideas has already been referred to several times: the prediction of flow velocities in powder-snow avalanches on steep slopes. Though the density differences in that case are due to suspensions of snow crystals in air, and can be quite large, the measured front velocities are in good agreement with the values obtained in laboratory-model experiments using salt and fresh water, as well as suspensions of solid particles in water. (Hopfinger & Beghin 1980 and Baines & Hopfinger 1984 have generalized the theory to include very large density differences. A discussion of this aspect is deferred to §8.) Turbidity currents produced by slumps of mud on the ocean floor have been successfully described in the same terms. The resulting deposits, and the channels cut by the currents, can be followed for great distances from shallow to deep water. Related phenomena on the surface of Mars have also been reviewed by Simpson (1982); it has been suggested that channels in the Martian surface could have been formed by gravity currents driven by dust particles suspended in the atmosphere.

Another type of downslope flow, which derives its energy from the density difference due to suspended particles of hot ash, is the nuée ardente, or pyroclastic flow, originating from an erupting volcano. Such flows can achieve speeds of up to 50 m s^{-1} over distances of several km. Because air is entrained into the top of the flow and heated, there is also upward convection associated with this downslope flow, which has recently been simulated in the laboratory by Huppert *et al.* (1986), using a mixture of methanol and ethylene glycol (MEG) flowing up under a sloping roof

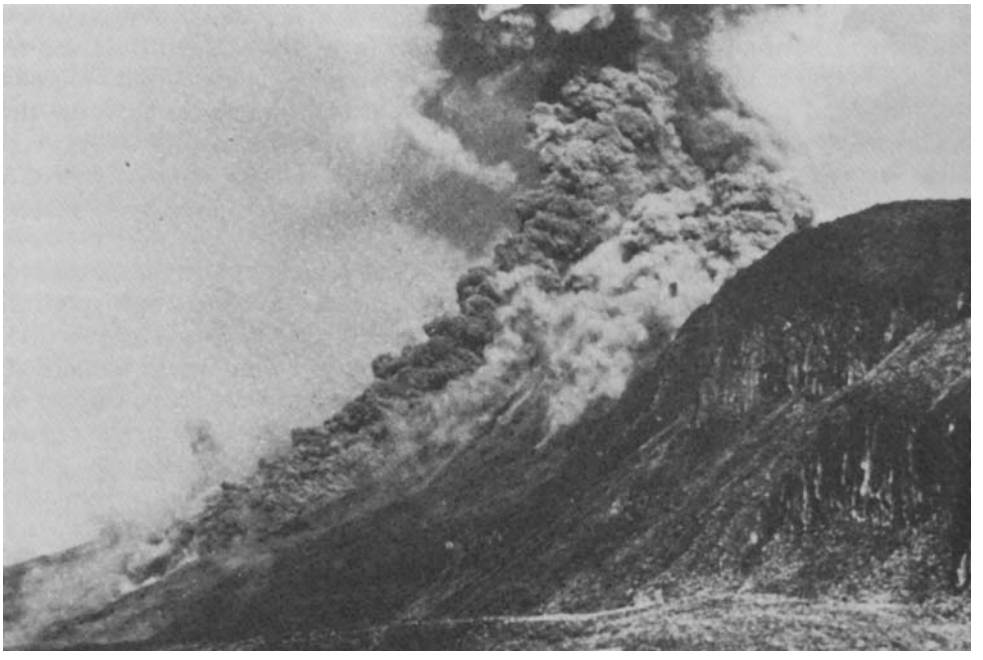

FIGURE 7. A nuée ardente, a downslope flow of hot ash, with a convecting cloud of heated air above it, formed during the 1975 eruption of Ngauruhoe in New Zealand. (See Nairn & Self 1978; photo by R. Foley.)

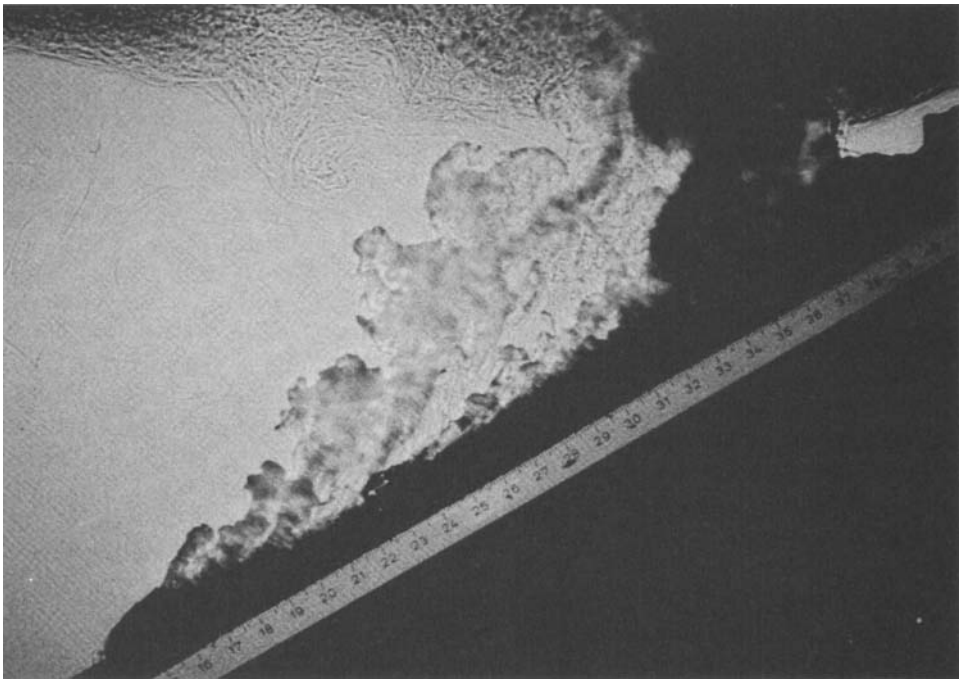

FIGURE 8. A laboratory model of a nuée ardente. The nonlinear density changes accompanying the mixing of a methyl alcohol/ethylene glycol mixture with water have been used to simulate the reversal of buoyancy due to entrainment and heating of the air above a downslope flow of hot ash. This photograph has been inverted to facilitate comparison with the natural phenomenon shown in figure 7. (After Huppert *et al.* 1986).

in water. The mixing behaviour of MEG and water is very nonlinear, so that intermediate mixtures can be denser than either original component. Thus as the light MEG flows along the slope and entrains water, a relatively dense intermediate mixture forms and convects away from the slope, so providing an inverted model of the natural phenomenon. The two are compared in figures 7 and 8. The results obtained so far for this laboratory analogue are mainly qualitative, but there is some indication that the downslope velocity of the front of model nuée ardentes is less than that of an ordinary gravity current. This is probably due to a combination of two effects: the extra drag caused by the upflow at the edge, and the decreasing downslope buoyancy flux associated with the density reversal.

7. Mixing across density interfaces

In this section it seems appropriate first to survey briefly the geophysical processes and applications before going on to describe the theories and laboratory experiments that have been developed in order to understand them. Well-mixed layers of nearly constant density often occur near boundaries in stratified fluids. The overall effect of the energy inputs near the ground or the sea surface, for example, is to produce a more homogeneous, turbulent surface layer, bounded by a region of increased density gradient – the inversion layer in the atmosphere, and the diurnal or seasonal thermocline in the ocean. This layer of high stability is only intermittently turbulent, and it acts as a barrier to the transport of mass and heat (and other properties such as moisture or salinity) out of the surface layer. The depth and composition of the well-mixed layer can, however, change because of entrainment into it through the interface, and a variety of processes which affect the entrainment must be understood before one can predict, for example, the depth of the oceanic mixed layer and the sea-surface temperature. Among the effects which need to be considered in turn are the nature of the surface energy sources (whether the mixing is due to the mechanical effects of the wind stress, or to convection), the influence these have, individually or in combination, on the motion in the surface layer, and finally the mechanism of entrainment at the interface itself.

The theoretical and laboratory studies described below are integral models, which treat the mixed layer as a single entity and are one-dimensional in depth. That is, the mixing is supposed to be uniform in the horizontal, though horizontal currents driven by a wind stress and variations in time of the input processes can be included, and some individual localized mixing processes will be discussed. There have been several fairly recent reviews of the development of these one-dimensional models and especially of their relevance to the ocean (Niiler & Kraus 1977; Sherman, Imberger & Corcos 1978; Turner 1981), which can be referred to for more details. Here, as in earlier sections, we use selected laboratory experiments to illustrate the principles involved, which again rely heavily on modifications of the entrainment assumption. The overall results will be described first, and then (in the following section) some more detailed experiments and theories which probe further into the fundamental mechanisms of turbulent entrainment in homogeneous and stratified fluids.

We consider now mechanical mixing processes, starting with the case where a constant stress τ_0 is applied at the surface (for example by the wind) but without any heat (i.e. buoyancy) flux. The associated velocity scale is the friction velocity v_*, defined by $\tau_0 = \rho_w v_*^2$. Suppose that at time t the well-mixed layer has depth h and a density step $\Delta\rho$ below it. A dimensional argument related to that used in (21)

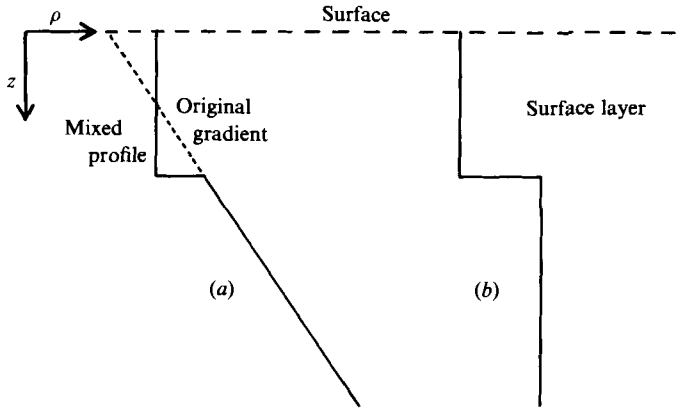

FIGURE 9. Sketch of the starting conditions for the two types of laboratory experiments used to model mixing due to surface energy inputs. (*a*) A linear density gradient: a step forms as the surface layer becomes well mixed. (*b*) Two homogeneous layers.

suggests that the entrainment velocity $U_e = \mathrm{d}h/\mathrm{d}t$ (which is equivalent to E_b, defined just before equation (13)) can be expressed in the form

$$\frac{U_e}{v_*} = E_*(Ri_*), \tag{25}$$

where Ri_* is an overall Richardson number based on the friction velocity, $Ri_* = gh\Delta\rho/\rho_w v_*^2 = C^2/v_*^2$, say. Note that there has been a subtle change in the entrainment assumption in this formulation, with the friction velocity replacing the mean velocity.

Two related laboratory experiments, by Kato & Phillips (1969) and Kantha, Phillips & Azad (1977), have modelled this process and tested (25), using respectively the starting conditions shown in figure 9(*a*,*b*). They both used an annular tank to eliminate end effects, and the stress τ_0 was applied through a rotating grid at the surface. (We note in passing a series of related experiments recently reported by Narimousa, Long & Kitaigorodskii (1986) from the same laboratory, which used a disk pump to drive the shear flow.) The first experiment started with a linear salinity gradient (buoyancy frequency N), and in that case the depth h is related to $\Delta\rho$ and N by

$$C^2 = \frac{gh\Delta\rho}{\rho_w} = \tfrac{1}{2}N^2h^2. \tag{26a}$$

In the second set of experiments the gradient was replaced by two layers of different density, and conservation of buoyancy in that case gives

$$C^2 = \frac{gh\Delta\rho}{\rho_w} = \text{const.} \tag{26b}$$

The difference is that C^2 and Ri_* are definitely increasing as the layer deepens in case (*a*), whereas they are constant in case (*b*).

It is significant that (25) does not collapse the data of these two sets of experiments on to a single curve: at a given Ri_* and h, E_* is a factor of two larger in the two-layer experiments than with a linear gradient. Price (1979) proposed that the rate of entrainment should be scaled instead with the mean velocity V of the layer (or more generally, the velocity difference (δV) across the intervace), $u_e/V = E(Ri_V)$, with Ri_V

also defined using V. When the data are replotted in this way (and proper corrections are made for sidewall friction), the data from the two experiments do agree, and the form of the deduced entrainment function $E(Ri_V)$ is close to that previously obtained by Ellison & Turner (1959) for gravity currents, and approximated by (23).

The formulation in terms of V implies that conservation of mean momentum is the most important constraint on entrainment in these experiments (and in the analogous oceanic case), and it is consistent with our earlier emphasis on the large-scale motions. Using the momentum equation $\mathrm{d}(hV)/\mathrm{d}t = v_*^2 = \text{const.}$ with the conservation of buoyancy relations (26) gives

$$E_* = \frac{u_e}{v_*} = nRi_V^{\frac{1}{2}} Ri_*^{-\frac{1}{2}}, \tag{27}$$

where

$$n = \begin{cases} \frac{1}{2} & \text{if } C^2 = \frac{1}{2}N^2h^2 \quad \text{(linear stratification)}, \\ 1 & \text{if } C^2 = \text{const.} \quad \text{(homogeneous layer)}. \end{cases}$$

Thus the observed factor-of-two difference in the entrainment rate E_* defined using v_* is also predicted by this model. The difference arises because, if Ri_V is to stay constant in the linearly stratified case as C^2 increases, the whole layer must be accelerated to the velocity $V = (C^2/Ri_V)^{\frac{1}{2}}$, not just the entrained fluid. In the two-layer case, on the other hand, the stress is only required to accelerate the entrained fluid to velocity V, which is constant.

Note that the use of V or δV as a velocity scale allows other physical processes to be incorporated into the calculation. For timescales such that the Earth's rotation is important, for instance, the momentum equation in rotating coordinates must be used to calculate δV for the oceanic mixed layer as a function of v_* (and also of h, the Coriolis parameter f and time). It can be shown that rotation dominates the shear at the base of the mixed layer for timescales comparable with half a pendulum day, and that δV is then proportional to v_*^2. It is thus not true that all velocity scales are equivalent, and certainly only in special circumstances is V proportional to v_*.

The second type of conceptual and laboratory model of mechanical-mixing effects considers the situation where there is no mean flow, and turbulent kinetic energy is produced at a plane surface on scales much less than the depth of the layer. A convenient way to study this case is to use a vertically oscillated grid of solid bars to generate the turbulence, and the first experiments designed to quantify this process were summarized by Turner (1973). There have been many more experiments since then, and some controversy over their interpretation, but a clearer picture seems now to have emerged. In evaluating the present state of this subject, and reviewing the earlier work, the paper of E & Hopfinger (1986) is particularly helpful. Figure 10 is reproduced from their paper.

This mixing rate across the density interface bounding the stirred layer can again be put in the form (25), with a Richardson number based on the density difference $\Delta\rho$ and appropriate velocity and length scales expressing the major balance of forces. Explicitly, Thompson & Turner (1975) suggested that in this case the scales used to define the overall Richardson number $Ri_0 = g\Delta\rho l_1/\rho u_1^2$ should be the integral lengthscale l_1 of the turbulence, and the r.m.s. value u_1 of the horizontal component of turbulent velocity, both measured near the interface. These are more appropriate than overall parameters such as the velocity of the stirrer and the layer depth h but l_1 and u_1 can be related to the latter in particular experiments. For grids of square bars, with a spacing $M/d = 5$, where M is the mesh width and d the bar size, Hopfinger & Toly (1976) showed that the available experimental results can be fitted

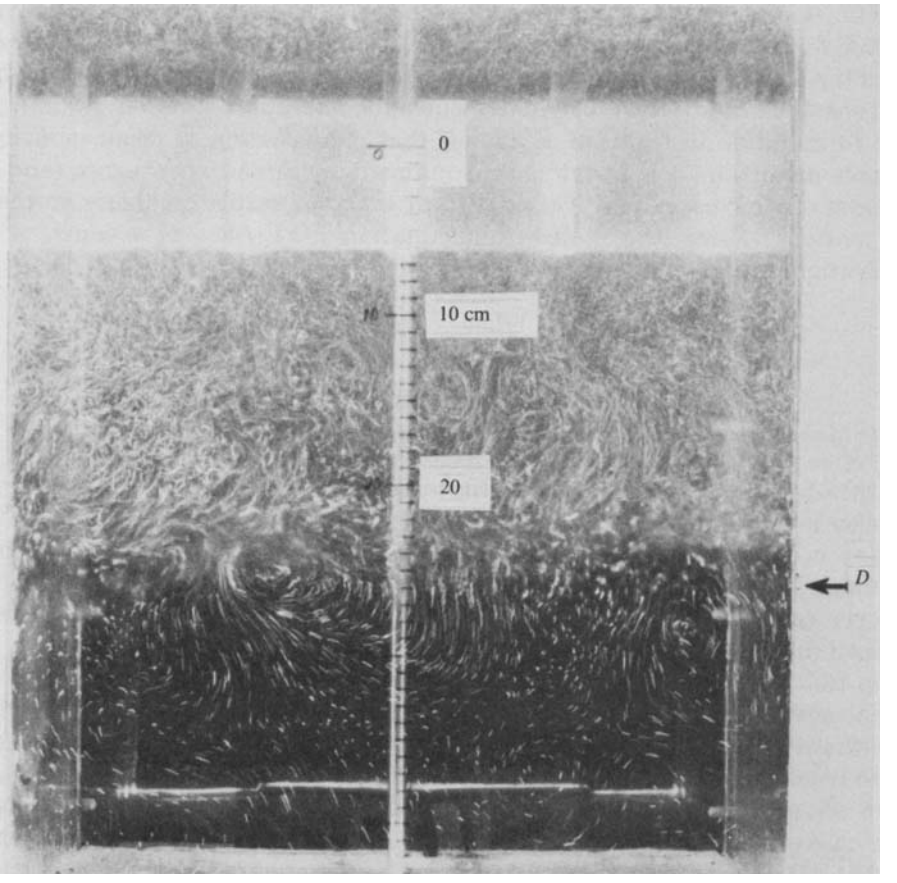

FIGURE 10. The stirring-grid experiment of E & Hopfinger (1986). This streak picture (exposure time 1 s) shows the well-mixed surface layer with large turbulent motions, and smaller internal-wave motions in a constant-gradient layer below the interface.

by $u_1/fS = CS^{\frac{1}{2}}M^{\frac{1}{2}}z^{-1}$, where f is the frequency of oscillation and S is the stroke, and C is a constant which is about 0.30. The most important part of this result is the z^{-1} decay of r.m.s. velocity with distance z from the grid midplane. The integral lengthscale l_1 increases linearly with distance z from the grid, with a constant of proportionality of about 0.10 when S/M is less than about 0.2. The typical Reynolds number $u_1 l_1/\nu$ in Thompson & Turner's (1975) experiment was ≈ 50, which was large enough for viscous effects to be negligible, and the value in subsequent experiments has been even larger.

Using these scales, the laboratory data are well described by the relation $u_e/l_1 = f(Ri_0, Pe)$ where $Pe = u_1 l_1/\kappa$ is a Péclet number based on u_1, l_1 and the molecular diffusivity κ. When $Ri_0 > 7$ and $Pe > 200$, which can be achieved in laboratory experiments using salinity differences, the explicit form obtained is

$$\frac{u_e}{u_1} = KRi_0^{-\frac{3}{2}}, \tag{28}$$

where K is a constant. In this limit, entrainment is controlled by non-diffusive processes, and according to Crapper & Linden (1974) the interface thickness h is then a nearly constant multiple of l_1 ($h = 1.5l_1$ approximately), though more recent work

suggests that it may decrease slowly with increasing Ri_0. Field measurements of temperature profiles through the base of the surface mixed layer in the ocean, however, often reveal interfaces much thinner than this, and current laboratory observations by E. J. List and collaborators (personal communication) have revealed the same features in oscillating-grid experiments. These are evidence for active mixing events which are sharpening the interface locally, and they suggest the need for caution in defining the thickness of an interface.

The mechanistic explanation for the $-\frac{3}{2}$-power law given by Linden (1973) still seems to be sound. By projecting vortex rings against an interface, he showed that mixing takes place during the recoil event, so that turbulent kinetic energy is made available for mixing at a rate set by the recoil velocity δ/τ_B, where δ is the penetration depth of the eddies $\delta \propto \bar{\rho} u_1^2/g\Delta\rho$ and $\tau_B \propto (\bar{\rho} l_1/g\Delta\rho)^{\frac{1}{2}}$ is the response time of the interfacial layer to disturbances of lengthscale l_1; it does not depend directly on the overturning timescale of the eddies. Equating the rate of supply of kinetic energy $\bar{\rho} u_1^2 \delta/\tau_B$ to the rate of change of potential energy $g\Delta\rho h \mathrm{d}h/\mathrm{d}t$ then gives $u_e/u_1 \propto Ri_0^{-\frac{3}{2}}$. Another significant result is the observation that entrainment of fluid (in one direction) into a mixed layer is independent of whether the other layer is stirred or not (though of course the flux entrainment velocity E_F as defined following (13*a*) will be doubled if both layers are stirred). This is because the mixing events on each side are so rare that they can be considered statistically independent.

E & Hopfinger (1986) have recently carried out a definitive set of measurements using both two-layer and constant-gradient systems, and have accurately confirmed the form (28) at high values of Ri_0 and Pe, with an exponent 1.54 ± 0.05 and $K \approx 3.8$. These measurements also verify the previously suggested frequency dependence, and they seem conclusively to discriminate against the deepening rates predicted by the $-\frac{7}{4}$-power law resulting from Long's (1978) phenomenological theory and tested by Fernando & Long (1983). The latter papers contain the suggestion that entrainment and mixing are caused by the generation and intermittent breaking of internal waves in the interfacial layer, which will have the same timescale as the recoil mechanism, but there are also other detailed assumptions which are evidently not borne out by the measurements of E & Hopfinger. It seems likely that the controversy generated by these different viewpoints will continue for some time.

At low Péclet numbers (< 200, which were obtained using temperature differences) but still with $Ri_0 > 7$, molecular diffusion affects the structure of the interface, and the entrainment relation is different because the turbulence is encountering a different density gradient locally. (The importance of including the effects of diffusion on the interfacial temperature gradient has been demonstrated by Denton & Wood 1981, who have studied convectively driven entrainment at low Pe.) There is now a diffusive core across the centre of the interface, and h/l increases as Pe is reduced (see figure 11). The mixing rate for heat found by Turner (1968) in this range of Pe was greater than that for salt, and the power-law dependence is now close to $u_e/u_1 \propto Ri_0^{-1}$. Though this is the form suggested by a simple energy argument (see below) it is probably due to a much more complicated interaction of diffusion and entrainment processes, and is not as fundamental as the $-\frac{3}{2}$-result.

At low values of Ri_0 (< 7) the entrainment rate becomes independent of Pe and all the experimental curves run together. As Ri_0 decreases, the entrainment rate 'flattens out' and depends less strongly on Ri_0. Though it is tempting to seek explanations for various power laws in different parameter ranges it is probably better to regard this as a continuous transition (cf. Narimousa *et al.* 1986). In this range of Ri_0, a turbulent eddy entering the interfacial layer tends to thicken the

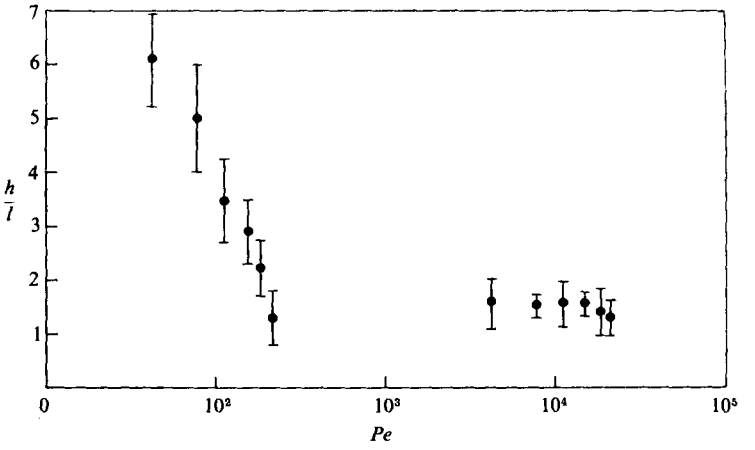

FIGURE 11. The non-dimensional mean interface thickness h/l plotted against the Péclet number Pe, for experiments in which the layers on both sides of the interface were stirred with oscillating grids (from Crapper & Linden 1974).

interface, rather than sharpening it as it does at high Ri_0 – there is an excess of mechanical energy, and both the stratification and diffusion become unimportant. Entrainment takes place by an engulfment process just as it does in a non-stratified fluid.

As Ri_0 increases, wave motions must be taken explicitly into account, both at the interface itself and in any stratified region adjoining a well-mixed layer, in any full explanation of the entrainment mechanism, and this aspect is discussed further in §8.3. However, the recent experiments of E & Hopfinger (1986) (with $Ri_0 > 7$) did not detect any difference in entrainment rates between two-layer experiments and those starting with a linear gradient. This suggests that energy radiated away from the interface by internal waves does not have a significant effect on the mixing or on the deepening rate of the upper mixed layer (contradicting a previous conclusion of Linden 1975). It may still be important, however, as a source of wave energy for the deep ocean, though the existence of a mean shear flow in the upper layer probably also has a significant influence on internal-wave generation.

The final group of processes to be considered here is related to the effects of buoyancy fluxes of both signs on the development of a mixed layer. When there is a net heat (buoyancy) input, at the sea surface for example, a stabilizing density gradient is set up, which has an inhibiting effect on the mixing by mechanical inputs, as discussed above. With a constant stabilizing buoyancy flux $B = \overline{g\rho' w'}/\bar{\rho}$ from above (i.e. a constant rate of heating right at the surface) and simultaneously a fixed rate of supply of kinetic energy, assumed to be proportional to u_*^3 where u_* is the friction velocity, there can be a balance between the mechanical energy and the work required to mix buoyant fluid downwards. The depth of the surface layer can then become steady while it continues to warm. This steady depth depends on u_*^3 and on the rate of decay of the turbulent kinetic energy with depth, as well as on B (Hopfinger & Linden 1982). The process involves *no* entrainment across the bounding interface below, across which there is an increasing density difference: all the turbulent energy either decays or is used in stirring buoyant fluid from the surface down to this depth and increasing the potential energy.

On the other hand when there is a net cooling at the sea surface, at night or during

the winter, convective motions can extend to the depth of the mixed layer and contribute to entrainment across the thermocline below. The extent to which the deepening is 'penetrative' or 'non-penetrative' – i.e. whether the process can be described as being one of 'entrainment' rather than just 'encroachment' into an existing density structure – has been a subject of debate. The question is also of importance in the complementary case of an atmospheric surface layer during conditions of strong heating, and the early work on this has been discussed by Deardorff, Willis & Stockton (1980), who have paid particular attention in their own laboratory experiments to the 'entrainment zone' itself, i.e. what we have previously loosely described as the interface.

The experiments of Deardorff *et al.* (1980) were conducted in water, with the stratification (either a step or a gradient above a well-mixed, thermally convecting layer) produced using temperature differences. The natural velocity to use in this case is the turbulent velocity scale for a convectively mixed layer of mean depth $\bar{h}$, defined by

$$w_* = [B\bar{h}]^{\frac{1}{3}}, \tag{29}$$

where B is now an unstable buoyancy flux. The corresponding overall Richardson number is then $Ri_* = g\bar{h}\Delta\rho/\rho w_*^2$. The observed entrainment rates over a range of Ri_* values in the laboratory experiments ($7 < Ri_* < 100$ which includes most of those to be expected for atmospheric or oceanic mixed layers) can be represented by

$$w_e/w_* = 0.25 Ri_*^{-1}. \tag{30}$$

In spite of the use of temperature differences to produce the stratification in these experiments, the Péclet number was high, in the terms used in the discussion of mechanical mixing. One might therefore have expected a $-\frac{3}{2}$-power law, according to the previous arguments, and this is not excluded by the scatter of the data, though (30) gives a somewhat better fit. There was no evidence for a reduction in mixing rate due to wave energy propagating into a gradient region outside the mixed layer. These laboratory experiments indicated that there was indeed true entrainment at the top of the mixed layer, i.e. a definite step (or region of larger gradient) was produced during mixing into a stratified fluid above, rather than a direct transition from the homogeneous layer to the original gradient (the definition of encroachment).

It remains to sketch how the ideas about entrainment and the laboratory measurements described above have been incorporated into time-dependent models of the oceanic thermocline or atmospheric inversion. Virtually all of these models are based on energy arguments, which balance the inputs of kinetic energy against changes in potential energy plus dissipation. Thus they largely ignore the evidence for the $Ri_0^{-\frac{3}{2}}$ dependence of mixing on Richardson number, and substitute the more convenient Ri_0^{-1} form instead, which also receives limited support from the experiments on convectively stirred layers (equation (30)). The most arbitrary feature is the parameterization of dissipation. It is generally assumed (or implied) that the energy available for entrainment is some fixed fraction of that produced by each type of source and that these are additive. Laboratory and field data obtained on occasions when just one process was acting alone are used to evaluate the constants of proportionality. This is the view taken by Fischer *et al.* (1979), for example, and they have been very successful in applying such a composite model to a wide range of mixing problems in reservoirs, with numerical constants fixed in advance of particular applications. There have been some well-documented and successful examples of the application of models developed from that of Kraus &

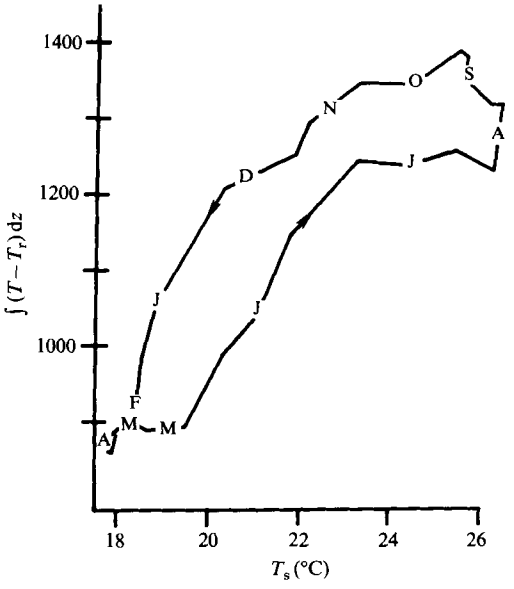

FIGURE 12. The heat content in the ocean surface layer as a function of surface temperature T_s derived from observations made at ocean weather station Echo. The heat content is integrated from the surface down to a standard reference level T_r; months are marked along the curve. (After Gill & Turner 1976).

Turner (1967), using a parameterization in terms of the surface wind stress and buoyancy flux with observed values of wind speed and radiation, to predict the time-dependent depth and temperature of the upper mixed layer of the ocean over periods of a few weeks.

Gill & Turner (1976) concluded that the Kraus–Turner model also works well on the seasonal timescale and, in particular, correctly reproduces the phase relationships between the dates of maximum heating, maximum surface temperature T_s and minimum depth. It predicts a realistic hysteresis loop in a plot of T_s versus heat content in agreement with observations such as those shown in figure 12. The best agreement with the observed sea-surface temperature is obtained, however, only when the theory is modified to allow potential energy to decrease, and the penetrative convective mixing to be zero, during the cooling period. The structure of the thermocline is also not very well represented by these integral models.

The need to make this kind of arbitrary change in the physical assumptions, in spite of the result suggested by the laboratory experiments of Deardorff *et al.* (1980), clearly indicates that something is lacking in our understanding of the entrainment process at least on a geophysical scale, and probably also at the fundamental level. But it is worth standing back again, as we did in §4 in discussing (15) for plume rise, to ask why the modified entrainment assumption relating the mixing to the Richardson number works as well as it does, in spite of the demonstrable inaccuracies in the formulation. It is particularly surprising that when the mixing is dominated by a few sporadic events, as it is at high Ri, the entrainment rate can be represented by a function of Ri based on mean quantities, rather than on some higher moments of the turbulence.

The length and velocity scales, and the density differences, vary widely between the laboratory models and geophysical flows. The results show that the entrainment

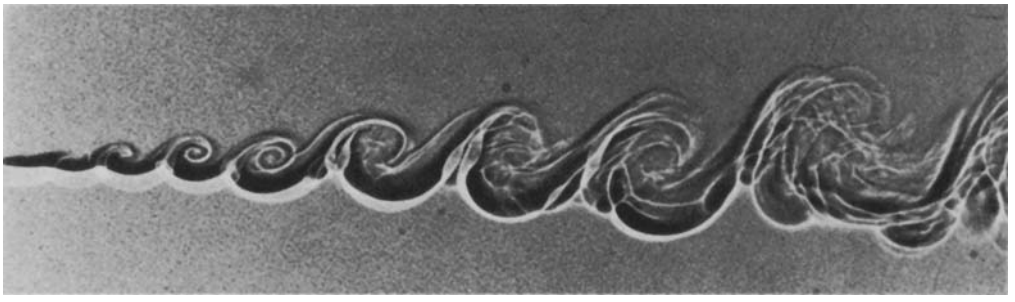

FIGURE 13. Spark-shadowgraph of a mixing layer between streams of helium (upper) and nitrogen (lower), showing the dominance of the large coherent structures. The experiment was conducted with the interface vertical, but the photo has been rotated by 90° for convenience of reproduction. (From Brown & Roshko 1974.)

velocity should first be scaled with a velocity representative of the large eddies near the entraining interface. The buoyancy–inertial force balance is contained in some form of Richardson number, which varies over several orders of magnitude in both the laboratory experiments and geophysical examples. The entrainment rate, relative to the reference velocity, is a strong function of the Richardson number, and it is this fact, rather than the precise functional dependence, which makes the overall predictions of the models so satisfactory, at least in relation to the accuracy of the present data. More sophisticated measurements will undoubtedly require more refined theories.

Thus we proceed to the more detailed discussion of the entrainment mechanisms in the next section, seeking a more fundamental understanding of these processes but recognizing at the same time that subtle differences between alternative models may not lead to an immediate improvement in practical prediction methods.

8. The mechanism of entrainment

8.1. *Homogeneous fluids*

Various studies of the physical processes involved in entrainment and mixing will now be considered briefly, first for a homogeneous fluid and then with density stratification. These theoretical and experimental examples have been chosen because of the light they shed on the fundamental processes, and on the problems requiring further work, not necessarily because of their direct applicability in the geophysical contexts which have guided the choice of topics in other sections.

The dominance of large-scale engulfment as the primary mechanism of entrainment, the basic postulate on which the entrainment formulation is based, receives strong support from recent studies of the constant-density mixing layer. Both laboratory and associated numerical work on turbulent flows, and in particular the shear layer between parallel streams, have become very sophisticated, and there is a rapidly growing body of relevant research. Coherent structures, in the form of orderly growing vortex motions, are now known to be intrinsic features of many turbulent flows; these have been studied visually (see figure 13), and using conditional sampling and averaging of hot-wire measurements. The reviews of Cantwell (1981) and Ho & Huerre (1984) can be consulted for fuller references and details of current work, but the results of just two of the groups active in this area will be used to illustrate the ideas.

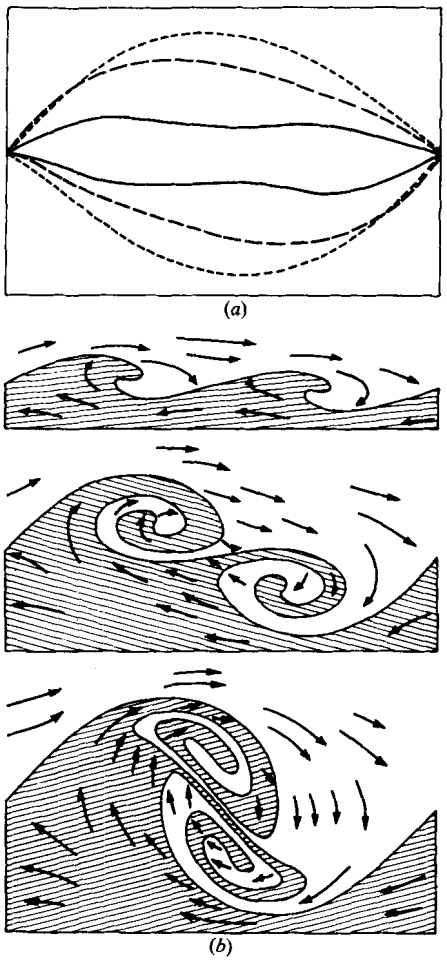

FIGURE 14. Two views of entrainment, according to Corcos & Sherman (1984). (*a*) The growth of the cat's eye at (dimensionless) times $\tau = 1.0, 2.0, 2.5$. (*b*) The visual record of 'engulfing', showing the successive positions of the interface at the same times, with fluid on one side shaded. The arrows are segments of streamlines, and are of arbitrary length.

In a series of papers, Corcos and his collaborators (e.g. Lin & Corcos 1984) have investigated deterministic, time-dependent numerical solutions of the Navier–Stokes equations describing the shear flow in a mixing layer at modest Reynolds numbers. They have successfully reproduced the observed roll-up of the vortex layer to form 'cat's-eye' vortices, and the subsequent subharmonic growth leading to pairing, which they show is preferentially two-dimensional. They clearly separate the concept of entrainment from that of the subsequent small-scale mixing and diffusion, and show that it is the initial 'engulfing' process associated with rolling-up and pairing of eddies that accounts for the observed linear time-averaged growth rates of the mixed layer. One definition of entrainment per unit span (from both sides of the layer) is just the rate of increase of the recirculating area of the cat's eye, and we note that the entering fluid is mostly irrotational. The shape of the cat's eye based on this view, and the calculated, more graphic record of the 'engulfing' at the corresponding times, are shown in figure 14, taken from Corcos & Sherman (1984).

Gaster, Kit & Wygnanski (1985) have used another approach to show that neither viscosity, nor small-scale turbulence, has a significant effect on the development of the very unstable waves that arise in mixing-layer shear flows. They have applied inviscid stability theory to the mean profile in a slowly diverging flow, and have reproduced the entire development of the wave amplitude observed in their experiments on a mixing layer which had similar mean-velocity profiles and a linear spread with distance. The measured cross-stream distribution of fluctuating velocity, associated with the large-scale organized structures, was also adequately described by this theory, in both magnitude and phase. The overall conclusion from all such studies is that the growth rate measured for fully developed turbulent mixing layers can be closely matched by growth rates deduced from calculations that take no account of small-scale turbulence. This gives powerful support to the entrainment hypothesis in its original form.

Theories that have emphasized the microscale 'entrainment interface' bounding the convoluted large-scale eddies should be mentioned. Phillips (1972) pursued the consequences of a description in which entrainment is regarded as essentially a viscous process, with the speed of advance of the interface bounding the turbulent fluid being proportional to the Kolmogorov velocity scale, $u_e \sim (\nu\epsilon_0)^{\frac{1}{4}}$ (where ν is the kinematic viscosity and ϵ_0 the local dissipation rate), augmented by micro-convolutions on scales comparable with the thickness of the interface itself. The more recent experimental results described above have shown that 'engulfment' of outer non-turbulent fluid is the dominant process, so that much of the 'entrainment interface' as defined by Phillips lies inside the region that has already been effectively entrained. The viscous diffusion of vorticity is thus important for the final digestion of external fluid into the turbulent flow and the evolution of the smaller-scale motions, but not in determining the overall rate of mixing. Some elements of this viscous diffusion mechanism could still be important for understanding mixing across density interfaces, at which the stabilizing buoyancy forces inhibit the formation of massive convolutions.

Another kind of viscous diffusion model of entrainment was discussed by Maxworthy (1972). He examined experimentally and theoretically the growth of vortex rings and the 'bubble' of fluid moving with them. As well as being of interest in the context of entrainment into thermals, they can be regarded as models of turbulent eddies thrusting out across a turbulent–laminar interface. His observations suggested the picture of a turbulent interface as an unsteady corrugated surface over which an outer irrotational fluid flows, and within which all of the vorticity is contained. As vorticity diffuses across the interface into the irrotational fluid, the fluid thus affected can no longer flow over the surface, but is entrained locally on the back side of corrugations. A laminar theory based on the incorporation of the diffusion layer growing to thickness of order $(\nu t')^{\frac{1}{2}}$, where t' is the time for a particle to traverse the distance round the 'bubble', was developed explicitly, with an allowance for the loss of some vorticity into the wake. This loss of vorticity (and of momentum) into the wake is even more significant in the case of turbulent vortex rings (Maxworthy 1974). Nevertheless, turbulent rings were observed to grow linearly with distance, with $\alpha \approx 0.01$, a result consistent with the entrainment assumption (16) which was used earlier for turbulent thermals. Note that in the case of the non-buoyant vortex ring the momentum (or impulse) is decreasing, rather than increasing as it does in a buoyant thermal or vortex ring. There is no result equivalent to (19), which relates the growth to the overall parameters rather than to the local turbulence, and clearly (19) cannot be used in the limit $F_* = 0$. The early hopes that these

growth models of simple vortex structures would shed more general light on the fundamental mechanisms of entrainment by the large eddies of turbulence do not seem to have been realized, again probably because of the dominant importance of the essentially inviscid engulfing motions. They do still, of course, retain their more direct interest in the context of entrainment into thermals and buoyant clouds.

8.2. *Large density differences*

Now seems an appropriate point to introduce a related topic, the effect of large density differences on entrainment (but first without any explicit buoyancy effects on the mixing). Batchelor (1954) discussed a few qualitative experiments on thermals with large density differences, produced by releasing increasingly light, miscible liquids into water. The smallest rate of spreading occurred for the lightest interior fluid (initial density 0.63 g/cm^3), and Batchelor attributed this to the effect of inertia. Explicitly, he suggested that as there is a smaller inertia associated with the turbulent interior motions, they therefore cannot penetrate so easily into the denser outer fluid and entrain it. The arguments leading to (19) have, however, raised the possibility that the lesser spread in these particular experiments might have been associated with the generation of a higher circulation during the acceleration from rest.

The overall effects of inertia have been incorporated explicitly into the theory of turbulent thermals in homogeneous surroundings by Escudier & Maxworthy (1973). This extends the entrainment theory developed from (16) to include arbitrarily large density differences, with the virtual mass of the environment and the inertia of the interior and exterior fluid both taken into account. They have considered the accelerating initial stage (where the entrainment assumptions are more questionable) and the later decelerating phase. As already noted in connection with (16), their modified mass-conservation equation still implies a linear angle of spread with distance at all times, equal to the entrainment coefficient. The momentum equation leads to

$$u = \frac{(\rho_\infty - \rho)}{(k\rho_\infty + \rho)} gt, \tag{31}$$

where u is the velocity at time t and g the acceleration due to gravity, ρ_∞ is the constant density of the environment and $\rho(t)$ the (local) density of the thermal, and k is the virtual-mass coefficient ($k = \frac{1}{2}$ for a sphere). It follows from (31) that light thermals will always have an initial acceleration larger than heavy ones. For example, for thermals very much lighter than the environment (so that $\rho_0/\rho_\infty \to 0$), and those twice as dense initially ($\rho_0/\rho_\infty = 2$), the ratio of the accelerations is 5, even though the density difference in the two cases is the same.

This approach leaves unanswered the question of any inertial effects on entrainment as such, and the processes that determine α. Baines & Hopfinger (1984) have used a local-entrainment argument to suggest that axisymmetric and two-dimensional thermals with large density differences should spread at a different angle in the early stages of the motion where the Boussinesq approximation is not valid. They base their mass-conservation equation on both the mass and the momentum of the fluid inside the thermal, with the density of the environment used as an explicit extra parameter because, they argue, this directly affects the mass via entrainment, whereas the interior density is already included in the other parameters. By this means, the physical basis of which is far from clear, they break away from the constraint of a constant linear spread, and deduce that the rate of growth of a heavy thermal is always larger, and of a light thermal always smaller, than the Boussinesq

case. This deduction receives limited support from experiments reported in the same paper, but the accelerating region, extending over only a few diameters, is too small for the measurements to be definitive. Our earlier discussion has suggested in fact that it is most unlikely that *any* entrainment argument based on similarity will be applicable to thermals in this region. A more detailed description of the accelerating stage is probably needed, in order to determine the circulation that is generated during this time and on which the whole of the subsequent behaviour depends.

A classic paper on plane turbulent mixing layers is that by Brown & Roshko (1974), a photograph from which is reproduced as figure 13. They explicitly addressed the question of the effect of large density differences on mixing rates, using streams of nitrogen and helium having a density ratio of 7. The flow was vertical, so that only the dynamic effects of the density difference were relevant, and no buoyancy forces entered, at least for the initial instability. (It remains a possibility, however, that buoyancy played a role once the vortices had wound around one another.) These spark-shadowgraph pictures were among the first to document the coherent structures, and the eddy roll-up and merging processes described earlier in this section. They compared cases where $\rho_1 U_1 = \rho_2 U_2$, and the mass flux was the same, or $\rho_1 U_1^2 = \rho_2 U_2^2$, so that the dynamic pressure was the same in both streams, with one where $\rho_1 U_1^2 = 49 \rho_2 U_2^2$. ($U_1/U_2 = \sqrt{7}$ in the latter two cases, but the two gases were in the opposite streams.) The mean rate of spread of the mixing layer with helium in the faster layer was approximately a factor of 2 greater than with nitrogen in the faster flow (with an intermediate rate of spreading for nearly equal-density gases, nitrogen and air). Mean-density and velocity profiles obtained for the same flows supported these visual measurements of the thinning of the mixing layer with increasing density on the high-speed side, though the spreading angle of the density profile was greater than that for the velocity. (A much greater decrease of spreading rate is observed when the faster stream is supersonic, but this has been attributed to a compressibility effect, which was not relevant in the experiments described above.)

There has been no physical explanation of these results, and very little work following them up, though it has been suggested by Chandrsuda *et al.* (1985) that they represent the behaviour of transitional flows, rather than fully turbulent mixing layers which rapidly become three-dimensional. (Most of the subsequent studies of mixing layers with density differences have concentrated on the buoyancy effects, using horizontal interfaces.) The dependence on the density difference is in conflict with the measurements and theoretical arguments developed for the convecting cloud or 'thermal' case, which led us to expect that a larger momentum associated with the denser flow would increase the entrainment rate. Though for most geophysical purposes the Boussinesq approximation gives adequate accuracy, the problem of mixing between fluids with large density differences is a fundamental one, which merits further attention.

8.3. *Stably stratified fluids*

When there is a region with a vertical density gradient or a horizontal density interface bounding a turbulent layer, different fundamental questions need to be considered. The picture of entrainment as simply the engulfment of external fluid by large eddies is no longer sufficient and, particularly when there is an interface, the dynamical situation is not just a small perturbation from turbulence in a homogeneous fluid. The response of the stratified region to the imposed turbulence, and the effect of this on the turbulent motions themselves, need to be taken into account. As the

Richardson number becomes large, or more explicitly, when $LN/U \gg 1$, where U and L are the velocity and length scales of the imposed turbulent motions and N is the buoyancy frequency of the stratified layer, the perturbations at the boundary between the turbulent and non-turbulent fluid become very small. The interfacial layer still contains small-scale shearing and wavelike motions and, as mentioned briefly in §7, entrainment takes place through a mechanism that can be thought of either as the recoil of the interface after it has been distorted by an impinging eddy, or as internal wave breaking. In either case wisps of fluid are ejected into the turbulent layer, and mixed thoroughly first by turbulence and finally by molecular diffusion.

This interaction between turbulence and the gradient region has been examined theoretically by Carruthers & Hunt (1986). They have considered initially the case of a homogeneous turbulent region adjoining a gradient region (with no density step), and have for the first time properly matched the turbulence to the wave motions in evaluating the velocity fluctuations near the interface. Their theory shows that eddies with frequencies of the same order as N are least affected by the stratification, and that the r.m.s. vertical velocity is greatest at the interface when $LN/U \approx 2$. The flux of energy into internal waves increases with this parameter, and is a maximum when $LN/U \approx 6$. This value has been identified by E & Hopfinger (1986) with the Richardson number above which the $Ri^{-\frac{3}{2}}$ power law is valid, i.e. the point at which the buoyancy timescale characteristic of eddy recoil becomes relevant, rather than the eddy-overturning timescale. In the limit of large stratification $N \to \infty$ the theory shows that the effect of the stable layer on the turbulent region is the same as that of a rigid surface, as previously studied by Hunt & Graham (1978). Near a solid wall, the fluctuations of normal velocity decrease monotonically, while the transverse velocity components become larger than their 'free-stream' values (an effect which can be visualized in terms of the flattening of eddies near the wall). McDougall (1979) made measurements through a density interface between two well-mixed layers which revealed some of the same features. His measurements showed in particular that the centre of the interface remained less active, suggesting that the turbulent eddies did not often penetrate to the centre but were halted and squashed at the edge of the interface.

The mechanism of entrainment by a single 'eddy' at a density interface has recently been considerably clarified by the experiments of Kumagai (1984), who has also consolidated and illuminated a lot of previous work. He considered the time evolution of a two-layer salt–fresh-water system when a dense plume of salt water was supplied at the free surface. The 'filling-box' process described by Baines & Turner (1969), which produces a stable stratification in the upper layer, is modified by the entrainment through the end of the plume which impinges on the interface. Kumagai also developed a theoretical model which takes both processes into account, and which describes well the observed vertical density profile, the time evolution of the density difference across the interface, and the time when the plume finally penetrates through the interface. Of special interest in the present context is the measured entrainment rate deduced from changes in thickness of the upper layer. This was expressed as a function of a Froude number Fr, which is equivalent in this case to the inverse square root of the interfacial Richardson number previously used in (28). The functional dependence is close to Fr^3 at small values of Fr (cf. $Ri_0^{-\frac{3}{2}}$ at large Ri_0), and the power gradually changes as Fr increases until the entrainment approaches a finite limit, just as in the grid-stirring experiments. This result therefore gives further support to the $-\frac{3}{2}$-power-law dependence of entrainment rate on

Richardson number in the high-Ri_0 limit, and indirectly (for another form of individual eddy impinging on the interface) to the eddy recoil mechanism proposed by Linden (1973) to explain it.

The same data have been interpreted by Kumagai (1984) in terms of the buoyancy flux across the interface, non-dimensionalized by the buoyancy flux in the plume. This can be shown to be equivalent to the ratio of the increase of potential energy due to the redistribution of the original (step) density profile to the potential energy made available by the buoyancy input in the plume, or alternatively to a kind of flux Richardson number R_f (if the energy in the plume is regarded as first converted to kinetic energy). This ratio varies systematically as a function of Fr, with a maximum of about 0.17 at $Fr = 0.46$ ($Ri_0 \approx 5$) and a sharp decrease at larger and smaller Froude numbers. Thus the energy supplied by the plume is used most efficiently at this particular intermediate Froude number. The lower efficiency at higher Fr is associated with large excursions of the interface, and a thickening as the condition for breakdown is approached, whereas at low Fr the 'recoil' mechanism is operating at a thin interface, which distorts less and less as Fr decreases. This maximum in the plots of energy ratio as a function of Fr, or R_f as a function of Ri_0, has been shown by Linden (1979) to be a general feature of a wide range of mechanical, as well as convective mixing processes. Referring back to the grid-stirring experiments (equation (28)), for example, R_f and Ri_0 are related by $R_f = (u_e/u)\,Ri_0$. Using a power-law fit to the experiments, $u_e/u \propto Ri_0^{-n}$ gives $R_f \propto Ri_0^{1-n}$. When $n < 1$ (at low Ri_0) R_f is an increasing function of Ri_0, whereas with $n = \frac{3}{2}$ (at high Ri_0) R_f is a decreasing function of Ri_0. The point where $n = 1$ corresponds to the maximum at which the simple overall energy argument applies.

As a final example of the effect of stratification on stability and mixing at an interface, consider an interfacial shear layer, across which there are sharp steps in both velocity and density. Energy considerations similar to those discussed above are also relevant in this case, and provide a limitation on the mixing which is not available for a shear layer in a homogeneous fluid. Experiments by Thorpe (1973) in a tilted tube containing two fluid layers with a sharp interface, and by Koop & Browand (1979) using two streams of fluid flowing together past a splitter plate, have carefully documented the nature of the instability. When the velocity and density profiles are similar, these flows become unstable when the minimum value of the gradient Richardson number falls below $\frac{1}{4}$ (whereas in the limit of zero density difference, all disturbances are unstable), and the fastest growing instability takes the form of regular Kelvin–Helmholtz 'billows'. The array of billows becomes unstable to subharmonic disturbances (much as it does in the case of the unstratified shear layer shown in figure 13) causing a rolling-up and merging of the original vortices.

The growth in the stratified case is, however, limited by an energy constraint. The system of vortices stops growing and then collapses, with much small-scale motion driven by convective overturning, accompanied by horizontal interleaving of mixed regions, and a rapid damping of the turbulence. Suppose that initial discontinuities of velocity ΔU and density $\Delta\rho$ are transformed by the process into linear gradients of velocity and density over the same interfacial depth δ (which is a good representation of what is observed in practice). Conserving mass and momentum, and equating the changes in kinetic and potential energies before and after the mixing events leads to

$$\delta_{\max} = \frac{2\rho_0(\Delta U)^2}{g\Delta\rho}. \tag{32}$$

The process is not perfectly efficient, however, and energy dissipation by viscosity leads to a much smaller observed maximum value for the thickness. The numerical factor varies with the initial Richardson number Ri of the interface, but Sherman *et al.* (1978) suggest using $\delta = 0.3\rho_0(\Delta U)^2/g\Delta\rho$ as a typical result for small values of Ri. This is in good agreement with the predictions of a theoretical model developed by Corcos & Sherman (1976), which considers the destruction of vorticity in the vortex cores by entrainment of stratified ambient fluid and the consequent production of a torque opposing the rotation.

There are two important implications of this result for the entrainment problem. First, the instability is self-limiting; unless the shear is increased, no further K–H instability can occur, since the interfacial Richardson number in the thickened state is higher than that required for instability. Secondly, the amount of vertical mixing that these interfacial K–H instabilities alone can account for is small. Only when there is an additional turbulence-generating mechanism in the homogeneous layers on each side of the interface will it be possible to transport material properties across the layers and also to produce the thinning of the interfaces which is required before further shear instabilities can develop. A broad range of scales of turbulent motion, in entraining shear flows or stirred layers, is thus probably an essential element in distinguishing 'entrainment' from purely interfacial instabilities.

9. The effect of viscosity differences on entrainment

Apart from the studies reported in §8.2, which examine the effect of large density differences, there has been little fundamental research on mixing between streams with very different physical properties. In this section we discuss a recently studied class of flows in which the extent of mixing between a turbulent fluid and its surroundings depends on the viscosity ratio between the two fluids. There has been some work reported in the engineering literature on mixing between very viscous fluids, including a discussion of viscosity differences, but much of this has been in relation to specific industrial stirring devices. The context for the experiments reported here is a geological one, the injection of a new pulse of magma into a magma chamber from below in the form of a 'fountain' (Campbell & Turner 1985, 1986), but the results have a wider significance.

When a fully turbulent fountain ($Re_1 \geqslant 400$) of fluid of low viscosity ν_1 is injected upwards into a less-dense fluid of higher viscosity (ν_2), the two fluids may mix thoroughly or not at all, depending on the relative magnitudes of the viscosity ratio and the input Reynolds number $Re_1 = wd/\nu_1$, where w is the mean velocity and d is the diameter of the input pipe. When the viscosities of the input and host fluid are comparable (with salt solution injected upwards into fresh water, for example) there is appreciable turbulent entrainment, so that as the fountain rises and falls back in an annular region surrounding the input pipe it builds up a stratified layer with a volume much greater than that of the added fluid (figure 15). However, when glycerol (with viscosity about 10^3 times that of water) is used as the host fluid, and a denser salt solution (K_2CO_3) is injected at a Reynolds number Re_1 of about 10^3, mixing is completely suppressed (figure 16). The internal flow in the fountain is still fully turbulent, but the boundaries with the upper viscous layer remain smooth, and the depth of the fluid building up at the bottom of the tank corresponds exactly to the rate of addition at the source, with no entrainment.

The external parameters in terms of which the mixing must be described are w, d, ν_1 and ν_2 (already introduced) and also $g' = g\Delta\rho/\rho$ where $\Delta\rho$ is the density excess

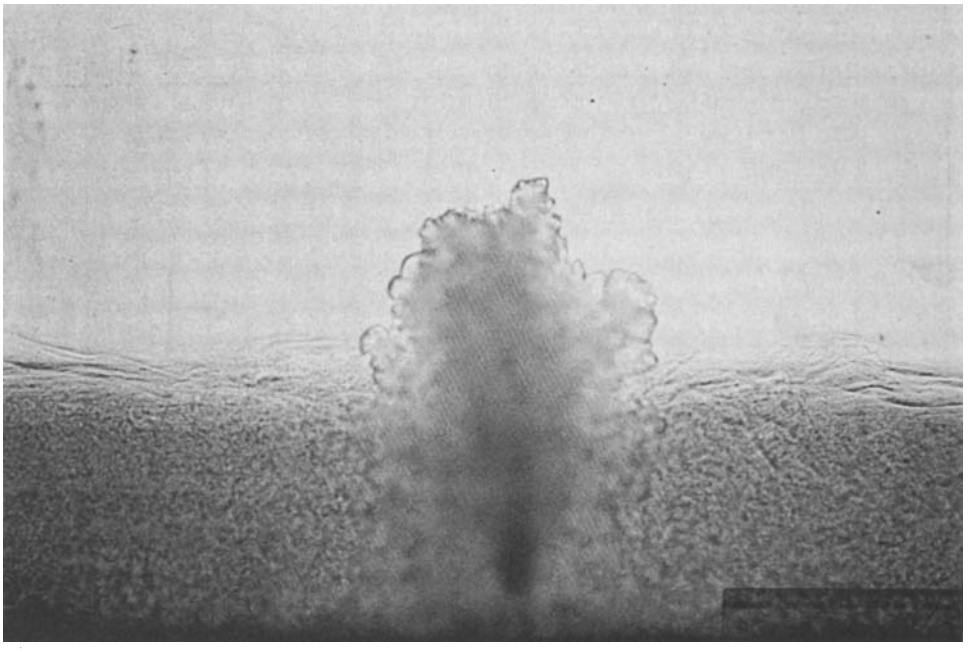

FIGURE 15. A 'fountain' formed by the input of dense salt solution at the bottom of a tank containing fresh water. Note the turbulent nature of the flow within the fountain, and the development of a stratified layer at the bottom of the tank.

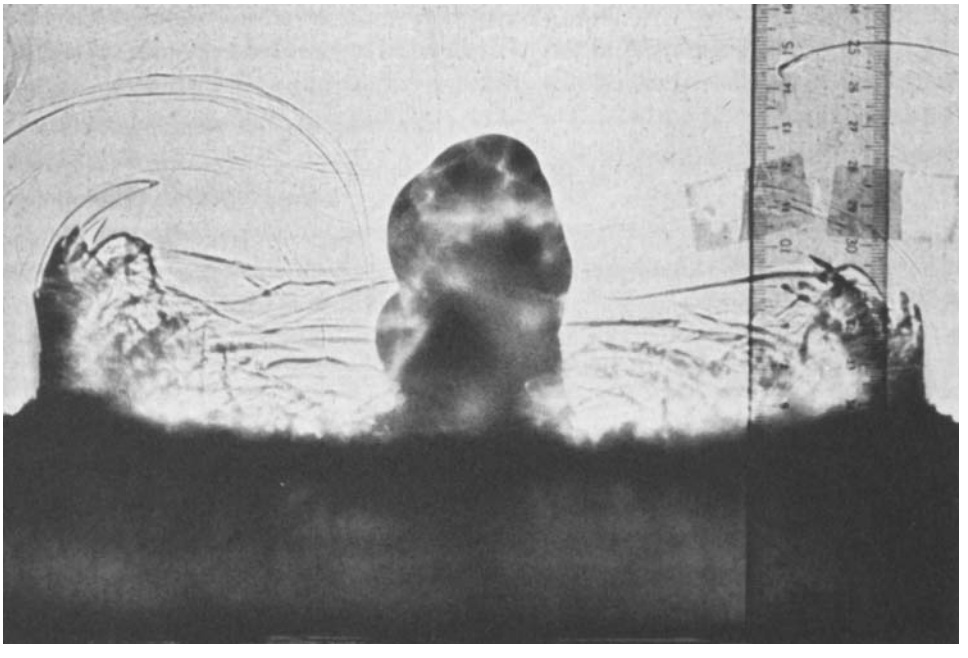

FIGURE 16. A fountain of K_2CO_3 solution injected upwards into much more viscous glycerine. Though the internal flow is turbulent, there is no mixing with the surrounding glycerine, so that the interface remains smooth. Compare with figure 15. (The annular plume at a larger radius is a double-diffusive effect, caused by the rapid diffusion of water across the interface into the glycerine layer.)

of the injected fluid. In addition to a Reynolds number and the viscosity ratio there is a third dimensionless parameter, which can be taken as an internal Froude number $w/(g'd)^{\frac{1}{2}}$. Alternatively one can use a formulation in terms of the overall source parameters (cf. (2) and (3)), the momentum flux $M \propto w^2d^2$ and the negative buoyancy flux $B \propto g'wd^2$, to define an overall lengthscale l and velocity scale v for a turbulent fountain:

$$l \propto M^{\frac{3}{4}}B^{-\frac{1}{2}}, \tag{33}$$

$$v \propto M^{-\frac{1}{4}}B^{\frac{1}{2}}. \tag{34}$$

The total height l_1 which fountains with $\nu_1 = \nu_2$ achieve before falling back is proportional to (33), and the constant of proportionality (c_1 say) has been evaluated by Turner (1966).

The product of (33) and (34) is independent of B, so that Re_1 is an appropriate Reynolds number to describe the whole flow, not only the input conditions. The fountain geometry thus seems a particularly useful one for a study of viscous effects (in contrast to a turbulent plume, say, for which the Reynolds number increases with distance). B enters only indirectly through its effect on the height of rise. In the experiments described below both Re_1 and $\Delta\rho$ and hence B were kept fixed for each series of experiments, and thus the dependence of entrainment on ν_2/ν_1 alone was tested in a nearly fixed geometry. In principle, the constant c_1 in (33) relating l_1 to the input parameters could also depend on the viscosity ratio, but no such direct viscous effect was detected. This implies that the decrease in upward momentum causing the flow in the fountain to reverse was always dominated by buoyancy acting on the inner turbulent flow and the interaction between the upward and downward streams of this inner flow, and not by entrainment of outer fluid.

The dramatic change of entrainment rate can be understood as follows. When a fluid of higher viscosity ν_2 surrounds the turbulent fountain, the host fluid can be entrained only when the inertial forces associated with the turbulence can distort or wrinkle the bounding surface. The limiting condition, at which the viscous and inertial forces are comparable at scale l in the outer fluid and viscosity inhibits any such distortion, can be expressed simply as $vl/\nu_2 \approx 1$, where l and v are defined by (33) and (34). This result can be derived in various (equivalent) ways, for instance by requiring that the Kolmogorov scales of the flow induced in the outer fluid be comparable with the scales v and l of the inner flow, or that the normal stresses generated by turbulence be comparable with the viscous stresses generated when the interface is deformed. Using again the result obtained from (33) and (34) that $vl \propto wd$, this relation implies that at high (turbulent) values of Re_1 the rate of mixing will be unaffected by any further reduction of ν_2 provided

$$Re_2 = \frac{wd}{\nu_2} > k, \tag{35}$$

where k is a constant. That is the criterion for uninhibited entrainment is determined by a Reynolds number based on the input parameters d and w of the fountain and the viscosity ν_2 of the outer fluid, and is independent of the viscosity ν_1 of the inflow. It can also be written in the more symmetrical form

$$Re_1 = \frac{wd}{\nu_1} > k\frac{\nu_2}{\nu_1}, \tag{36}$$

which predicts that as the viscosity ratio increases, the inflow Reynolds number must increase in proportion if mixing is to remain possible.

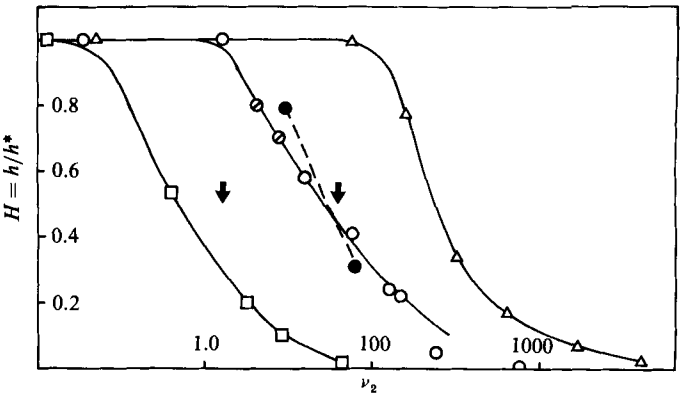

FIGURE 17. The results of 'fountain' experiments carried out using a fixed nozzle size and three input rates, corresponding to the different symbols: △, wd = 68 cm^2 s^{-1}, $\Delta\rho$ = 0.10 g cm^{-3}; ○, ●, ⊘ wd = 18 cm^2 s^{-1}, $\Delta\rho$ = 0.05 g cm^{-3}; □, wd = 3.9 cm^2 s^{-1}, $\Delta\rho$ = 0.0020 g cm^{-3}. The normalized entrainment $H(= h/h^*)$ is plotted against the kinematic viscosity ν_2 of the host fluid in centistokes, on a logarithmic scale. (See text for more details.)

These theoretical relations were used to interpret the results of three series of experiments, conducted for three fixed values of wd and $\Delta\rho$; the latter was chosen to give an experimentally convenient height of rise of the fountains. The total amount of fluid supplied, recorded as h_1, the height of the column of liquid added to the rectangular tank, was also kept fixed in each series. The 'entrainment height' h was defined as the difference between h_1 and the height h_m of the mixed or hybrid layer at the bottom of the tank. The maximum entrainment height h^* in each series, corresponding to the minimum value of ν_2, at which the outer fluid had no effect on reducing entrainment, was used to normalize the results.

The results of the three series of experiments with different values of wd are shown in figure 17, plotted as $H = h/h^*$ against ν_2 in each case. The following features give clear support to (35). For each value of wd, there is a critical value of ν_2, ($= \nu_2^c$ say) below which changes of viscosity of the host fluid have no influence on mixing. When $\nu_2 > \nu_2^c$ there is a rapid fall in the entrainment rate, which is controlled by ν_2 in this range; the rate is halved at a value corresponding to $k = 30$, and entrainment becomes negligible when $\nu_2 \gtrsim 10\nu_2^c$. The higher the value of wd, the higher is the value of ν_2 at which the viscosity of the host fluid first influences entrainment. If the 'entrainment midpoint' for the curve of highest input Reynolds number is scaled to the conditions of the other two experiments, the arrows mark the corresponding viscosities at which the entrainment is predicted (using (35) with $k = 30$) to fall to half their maximum values. The displacement of these arrows from the experimental curves is a measure of the direct effect of ν_1 in reducing entrainment, and the increasing disagreement at lower wd-values indicates a real effect of low Re_1, which has been documented in a further series of experiments.

It is to be expected that the principles established in this study will be more generally applicable to other turbulent flows surrounded by more viscous fluids, though comparable detailed results still need to be obtained for plumes, for example. For the particular geological application which motivated the 'fountain' study the conclusions are already very clearcut, however. If a primitive basaltic magma is injected into a chamber containing fractionated basaltic magma, the viscosity of both magmas will be low and not very different. The flow will be turbulent unless

the feeder pipes are very small, and the two magmas will mix readily. However, if basaltic magma is injected into a much more viscous silicic melt, little or no mixing will occur, except in the uncommon situation where the feeder dyke is several hundreds of metres wide.

10. Conclusions

Many different kinds of entraining flows have been surveyed in this paper, and the entrainment assumption has been shown to be useful in diverse contexts and over a wide range of scales. At several points we have paused to assess why it works so well in particular cases, but in this final section let us look again at the whole range of flows treated, picking out some common features and some unresolved problems.

The most successful and best-understood application is the entrainment into free turbulent flows such as jets or plumes. In these flows, the mixing is dominated by the mechanism of engulfment of external fluid by large eddies having velocity and length scales determined by the mean flow, and the underlying similarity assumption is likely to remain valid, even when the surroundings are stratified. The density differences are small, and the entraining boundaries are nearly vertical, so that buoyancy effects do not enter the problem. The recent more fundamental work on mixing across shear layers gives strong support to this picture, and explains why smaller-scale turbulence and viscous diffusion of vorticity need not be taken explicitly into account in describing the entrainment.

Turbulent thermals or buoyant vortex rings are in a special category, for which it is not clear that the concept of entrainment is appropriate at all. The rate of spread with height, and therefore the rate of incorporation of fluid moving with the buoyant element, are determined by the overall buoyancy and circulation, which can be set independently at the source and remain constants of the motion (in homogeneous surroundings). It may however be possible to define an appropriate velocity scale, related to these parameters, which would again justify the use of an entrainment assumption. The extent to which the small-scale turbulent motions in the buoyant core or the accompanying fluid are determined by the large-scale motion also needs to be examined further.

The entrainment concept has been extended to several different situations in which some other physical process, not simply engulfment by large eddies, dominates the rate of transfer across an interface. When there is a density step, with or without a mean shear flow, the most important additional parameter on which entrainment depends is a Richardson number based on the density difference and the velocity and length scales of the largest turbulent motions near the interface, i.e. a measure of the balance between inertial and buoyancy forces. It is the response of the fluid *outside* the turbulent region that determines the rate of entrainment in this case, and there are strong energy constraints on the mixing. The imposition of a velocity at an entraining interface is only the first part of the whole physical picture, which has been seen to involve a wavelike recoil of the interfacial region, and mixing by motions on different scales.

In a similar way, the ability of a turbulent flow to entrain a more viscous fluid outside it depends on the response of the external fluid. Inertial forces in the turbulent flow must be able to generate sufficiently large normal stresses in the surrounding fluid to overcome the viscous stresses and allow the interface to deform in the manner necessary for mixing. It seems likely that mixing between fluids of very different density might be amenable to an analogous approach, in which a turbulent

flow on one side of an interface is regarded as given, and the response of very much denser (or less dense) fluid outside the boundary calculated. The experimental and theoretical evidence on this point is, however, the most contradictory and least satisfactory of any of the results discussed in this paper. Part of the difficulty arises perhaps from the 'thermal' geometry in which some of the work has been done, and which leads to the ambiguity summarized above, between entrainment and the expansion set by the overall flow parameters. It should be possible to devise an experimental geometry that would give a clear answer to this question, and thereby shed further light on the entrainment mechanism in general. But we should note again in conclusion that the case of large density difference is of limited practical significance for most geophysical applications, in which the density differences rapidly become small enough for the Boussinesq approximation to be valid.

I am grateful to R. W. Griffiths, J. C. R. Hunt, H. E. Huppert, G. N. Ivey and P. F. Linden for their helpful comments on an earlier draft of this paper.

REFERENCES

BATCHELOR, G. K. 1954 Heat convection and buoyancy effects in fluids. *Q. J. R. Met. Soc.* **80**, 339–358.

BAINES, W. D. & HOPFINGER, E. J. 1984 Thermals with large density differences. *Atmos. Environ.* **18**, 1051–1057.

BAINES, W. D. & TURNER, J. S. 1969 Turbulent buoyant convection from a source in a confined region. *J. Fluid Mech.* **37**, 51–80.

BRIGGS, G. A. 1969 *Plume Rise.* U.S. Atomic Energy Commission Critical Review Series. 81 pp.

BRITTER, R. E. & LINDEN, P. F. 1980 The motion of the front of a gravity current travelling down an incline. *J. Fluid Mech.* **99**, 531–543.

BROWN, G. L. & ROSHKO, A. 1974 On density effects and large structure in turbulent mixing layers. *J. Fluid Mech.* **64**, 775–816.

CAMPBELL, I. H. & TURNER, J. S. 1985 Turbulent mixing between fluids with different viscosities. *Nature* **313**, 39–42.

CAMPBELL, I. H. & TURNER, J. S. 1986 The influence of viscosity on fountains in magma chambers. *J. Petrol.* **27**, 1–30.

CAMPBELL, I. H., MCDOUGALL, T. J. & TURNER, J. S. 1984 A note on fluid dynamic processes which can influence the deposition of massive sulfides. *Econ. Geol.* **79**, 1905–1913.

CAMPBELL, I. H., NALDRETT, A. J. & BARNES, S. J. 1983 A model for the origin of the platinum-rich sulfide horizons in the Bushveld and Stillwater Complexes. *J. Petrol.* **24**, 133–165.

CANTWELL, B. J. 1981 Organized motion in turbulent flow. *Ann. Rev. Fluid Mech.* **13**, 457–515.

CARRUTHERS, D. J. & HUNT, J. C. R. 1986 Velocity fluctuations near an interface between a turbulent region and a stably stratified layer. *J. Fluid Mech.* **165**, 475–501.

CHANDRSUDA, C., MEHTA, R. D., WEIR, A. D. & BRADSHAW, P. 1978 Effect of free-stream turbulence on large structure in turbulent mixing layers. *J. Fluid Mech.* **85**, 693–704.

CHU, V. H., SENIOR, C. & LIST, E. J. 1981 Transition from a turbulent jet into a turbulent plume. *ASME Conference, Boulder, Colorado, June 1981.*

CORCOS, G. M. & SHERMAN, F. S. 1976 Vorticity concentrations and the dynamics of unstable free shear layers. *J. Fluid Mech.* **73**, 241–264.

CORCOS, G. M. & SHERMAN, F. S. 1984 The mixing layer: deterministic models of a turbulent flow. Part 1. Introduction and the two-dimensional flow. *J. Fluid Mech.* **139**, 29–65.

CRAPPER, P. F. & LINDEN, P. F. 1974 The structure of turbulent density interfaces. *J. Fluid Mech.* **65**, 45–63.

CRAWFORD, T. V. & LEONARD, A. S. 1962 Observations of buoyant plumes in calm stably stratified air. *J. Appl. Meteorol.* **1**, 251–256.

DEARDORFF, J. W., WILLIS, G. E. & STOCKTON, B. H. 1980 Laboratory studies of the entrainment zone of a convectively mixed layer. *J. Fluid Mech.* **100**, 41–64.

DENTON, R. A. & WOOD, I. R. 1981 Penetrative convection at low Péclet number. *J. Fluid Mech.* **113**, 1–21.

E, X. & HOPFINGER, E. J. 1986 On mixing across an interface in stably stratified fluid. *J. Fluid Mech.* **166**, 227–244.

ELLISON, T. H. & TURNER, J. S. 1959 Turbulent entrainment in stratified flows. *J. Fluid Mech.* **6**, 423–448.

ESCUDIER, M. P. & MAXWORTHY, T. 1973 On the motion of turbulent thermals. *J. Fluid Mech.* **61**, 541–552.

FERNANDO, H. J. S. & LONG, R. R. 1983 The growth of a grid-generated turbulent mixing layer in a two-fluid system. *J. Fluid Mech.* **133**, 377–395.

FISCHER, H. B., LIST, E. J., KOH, R. C. Y., IMBERGER, J. & BROOKS, N. H. 1979 *Mixing in Inland and Coastal Waters.* Academic. 483 pp.

GASTER, M., KIT, E. & WYGNANSKI, I. 1985 Large-scale structures in a forced turbulent mixing layer. *J. Fluid Mech.* **150**, 23–39.

GILL, A. E. & TURNER, J. S. 1976 A comparison of seasonal thermocline models with observation. *Deep-Sea Res.* **23**, 391–401.

GORSHKOV, G. S. 1959 Gigantic eruption of the Volcano Bezymianny. *Bull. Volcanol.* **20**, 77–109.

HO, C.-M. & HUERRE, P. 1984 Perturbed free shear layers. *Ann. Rev. Fluid Mech.* **16**, 365–424.

HOPFINGER, E. J. 1983 Snow avalanche motion and related phenomena. *Ann. Rev. Fluid Mech.* **15**, 47–76.

HOPFINGER, E. J. & BEGHIN, P. 1980 Buoyant clouds appreciably heavier than the ambient fluid on sloping boundaries. In *Proc. 2nd Intl. IAHR Symp. on Stratified Flows, Trondheim*, pp. 495–504.

HOPFINGER, E. J. & LINDEN, P. F. 1982 Formation of thermoclines in zero-mean-shear turbulence subjected to a stabilizing buoyancy flux. *J. Fluid Mech.* **114**, 157–173.

HOPFINGER, E. J. & TOLY, J. A. 1976 Spatially decaying turbulence and its relation to mixing across density interfaces. *J. Fluid Mech.* **78**, 155–175.

HUNT, J. C. R. & GRAHAM, J. M. R. 1978 Free stream turbulence near plane boundaries. *J. Fluid Mech.* **84**, 209–235.

HUNT, J. C. R., ROTTMAN, J. W. & BRITTER, R. E. 1983 Some physical processes involved in the dispersion of dense gases. In *Proc. IUTAM Symp. on Atmospheric Dispersion of Heavy Gases and Small Particles, Delft* (ed. G. Oomes & H. Tennekes), pp. 361–395. Springer.

HUPPERT, H. E., TURNER, J. S., CAREY, S. N., SPARKS, R. S. J. & HALLWORTH, M. A. 1986 A laboratory simulation of pyroclastic flows down slopes. *J. Volcanol. Geotherm. Res.* (in press).

KANTHA, L. H., PHILLIPS, O. M. & AZAD, R. S. 1977 On turbulent entrainment at a stable density interface. *J. Fluid Mech.* **79**, 753–768.

KATO, H. & PHILLIPS, O. M. 1969 On the penetration of a turbulent layer into stratified fluid. *J. Fluid Mech.* **37**, 643–665.

KOOP, C. G. & BROWAND, F. K. 1979 Instability and turbulence in a stratified fluid with shear. *J. Fluid Mech.* **93**, 135–159.

KRAUS, E. B. & TURNER, J. S. 1967 A one-dimensional model of the seasonal thermocline. II. The general theory and its consequences. *Tellus* **19**, 98–106.

KUMAGAI, M. 1984 Turbulent buoyant convection from a source in a confined two-layered region. *J. Fluid Mech.* **147**, 105–131.

LIN, S. J. & CORCOS, G. M. 1984 The mixing layer: deterministic models of a turbulent flow. Part 3. The effect of plane strain on the dynamics of streamwise vortices. *J. Fluid Mech.* **141**, 139–178.

LINDEN, P. F. 1973 The interaction of a vortex ring with a sharp density interface: a model for turbulent entrainment. *J. Fluid Mech.* **60**, 467–480.

LINDEN, P. F. 1975 The deepening of a mixed layer in a stratified fluid. *J. Fluid Mech.* **71**, 385–405.

LINDEN, P. F. 1979 Mixing in stratified fluids. *Geophys. Astrophys. Fluid Dyn.* **13**, 3–23.

LIST, E. J. 1982 Turbulent jets and plumes. *Ann. Rev. Fluid Mech.* **14**, 189–212.

LIST, E. J. & IMBERGER, J. 1973 Turbulent entrainment in buoyant jets. *Proc. ASCE, J. Hydraul. Div.* **99**, 1461–1474.

LONG, R. R. 1978 A theory of mixing in a stably stratified fluid. *J. Fluid Mech.* **84**, 113–124.

LONGUET-HIGGINS, M. S. & TURNER, J. S. 1974 An 'entraining plume' model of a spilling breaker. *J. Fluid Mech.* **63**, 1–20.

MAXWORTHY, T. 1972 The structure and stability of vortex rings. *J. Fluid Mech.* **51**, 15–32.

MAXWORTHY, T. 1974 Turbulent vortex rings. *J. Fluid Mech.* **64**, 227–239.

MCDOUGALL, T. J. 1979 Measurements of turbulence in a zero-mean-shear mixed layer. *J. Fluid Mech.* **94**, 409–431.

MORTON, B. R. 1957 Buoyant plumes in a moist atmosphere. *J. Fluid Mech.* **2**, 127–144.

MORTON, B. R. 1959 Forced plumes. *J. Fluid Mech.* **5**, 151–163.

MORTON, B. R., TAYLOR, G. I. & TURNER, J. S. 1956 Turbulent gravitational convection from maintained and instantaneous sources. *Proc. R. Soc. Lond.* A **234**, 1–23.

NAIRN, I. A. & SELF, S. 1978 Explosive eruptions and pyroclastic avalanches from Ngauruhoe in February 1975. *J. Volcanol. Geotherm. Res.* **3**, 39–60.

NARIMOUSA, S., LONG, R. R. & KITAIGORODSKII, S. A. 1986 Entrainment due to turbulent shear flow at the interface of a stably stratified fluid. *Tellus* **38A**, 76–87.

NIILER, P. P. & KRAUS, E. B. 1977 One-dimensional models of the upper ocean. In *Modelling and Prediction of the Upper Layers of the Ocean* (ed. E. B. Kraus), pp. 143–172. Pergamon.

PHILLIPS, O. M. 1972 The entrainment interface. *J. Fluid Mech.* **51**, 97–118.

PRICE, J. F. 1979 On the scaling of stress-driven entrainment experiments. *J. Fluid Mech.* **90**, 509–529.

RICOU, F. P. & SPALDING, D. B. 1961 Measurements of entrainment by axisymmetric turbulent jets. *J. Fluid Mech.* **11**, 21–32.

SHERMAN, F. S., IMBERGER, J. & CORCOS, G. M. 1978 Turbulence and mixing in stably stratified waters. *Ann. Rev. Fluid Mech.* **10**, 267–288.

SIMPSON, J. E. 1982 Gravity currents in the laboratory, atmosphere, and ocean. *Ann. Rev. Fluid Mech.* **14**, 213–234.

SPARKS, R. S. J. 1986 The dimensions and dynamics of volcanic eruption columns. *Bull. Volcanol.* **48**, 3–15.

SQUIRES, P. & TURNER, J. S. 1962 An entraining jet model for cumulonimbus updraughts. *Tellus* **14**, 422–434.

THOMPSON, S. M. & TURNER, J. S. 1975 Mixing across an interface due to turbulence generated by an oscillating grid. *J. Fluid Mech.* **67**, 349–367.

THORPE, S. A. 1973 Turbulence in stably stratified fluids: a review of laboratory experiments. *Boundary-Layer Met.* **5**, 95–119.

TURNER, J. S. 1957 Buoyant vortex rings. *Proc. R. Soc. Lond.* A **239**, 61–75.

TURNER, J. S. 1960 A comparison between buoyant vortex rings and vortex pairs. *J. Fluid Mech.* **7**, 419–432.

TURNER, J. S. 1962 The starting plume in neutral surroundings. *J. Fluid Mech.* **13**, 356–368.

TURNER, J. S. 1963 Model experiments relating to thermals with increasing buoyancy. *Q. J. R. Met. Soc.* **89**, 62–74.

TURNER, J. S. 1966 Jets and plumes with negative or reversing buoyancy. *J. Fluid Mech.* **26**, 779–792.

TURNER, J. S. 1968 The influence of molecular diffusivity on turbulent entrainment across a density interface. *J. Fluid Mech.* **33**, 639–656.

TURNER, J. S. 1973 *Buoyancy Effects in Fluids.* Cambridge University Press, 367 pp.

TURNER, J. S. 1981 Small-scale mixing processes. In *Evolution of Physical Oceanography* (ed. B. A. Warren & C. Wunsch), pp. 236–262. MIT Press.

WILSON, L., SPARKS, R. S. J., HUANG, T. C. & WATKINS, N. D. 1978 The control of volcanic column heights by eruption energetics and dynamics. *J. Geophys. Res.* **83**, 1829–1836.